



HAL
open science

Astrochronology of the Aptian stage and evidence for the chaotic orbital motion of Mercury

Guillaume Charbonnier, Slah Boulila, Jorge Spangenberg, Jean Vermeulen,
Bruno Galbrun

► **To cite this version:**

Guillaume Charbonnier, Slah Boulila, Jorge Spangenberg, Jean Vermeulen, Bruno Galbrun. Astrochronology of the Aptian stage and evidence for the chaotic orbital motion of Mercury. *Earth and Planetary Science Letters*, 2023, 610, pp.118104. 10.1016/j.epsl.2023.118104 . hal-04071484

HAL Id: hal-04071484

<https://hal.science/hal-04071484>

Submitted on 19 Oct 2023

HAL is a multi-disciplinary open access archive for the deposit and dissemination of scientific research documents, whether they are published or not. The documents may come from teaching and research institutions in France or abroad, or from public or private research centers.

L'archive ouverte pluridisciplinaire **HAL**, est destinée au dépôt et à la diffusion de documents scientifiques de niveau recherche, publiés ou non, émanant des établissements d'enseignement et de recherche français ou étrangers, des laboratoires publics ou privés.

Charbonnier G., Boulila S., Spangenberg J.E., Vermeulen J., Galbrun B. (2023). Astrochronology of the Aptian stage and evidence for the chaotic orbital motion of Mercury. *Earth Planet. Sci. Lett.*, vol. 610, 118104. <https://doi.org/10.1016/j.epsl.2023.118104>

Astrochronology of the Aptian stage and evidence for the chaotic orbital motion of Mercury

Guillaume Charbonnier^{1*}, Slah Boulila^{1,2}, Jorge E. Spangenberg³,
Jean Vermeulen[†], Bruno Galbrun¹

¹ Sorbonne Universités, CNRS, Institut des Sciences de la Terre-Paris, IStEP, F-75005 Paris, France.

² ASD, IMCCE-CNRS UMR 8028, Observatoire de Paris, PSL Research University, Sorbonne Université, 77 avenue Denfert-Rochereau, 75014 Paris, France.

³ Institute of Earth Surface Dynamics, University of Lausanne, Géopolis, CH-1015 Lausanne, Switzerland.

* Corresponding author.

E-mail address: guillaume.charbonnier@sorbonne-universite.fr

† Deceased August 21, 2021.

Abstract

The Aptian stage, between ~113 and ~121 million years ago (Ma), was punctuated by a succession of Oceanic Anoxic Events (OAEs), recording extreme global warmings, dramatic expansions of the ocean's oxygen minimum zones, along with perturbations to the biotic and carbon cycles. However, the chronology of the Aptian stage is poorly constrained, impacting the duration and timing of OAEs. Using a greatly expanded sedimentary composite record (380 m) of key outcropping sections in the Vocontian Basin (SE France) combined with available radiometric dates and correlations to a set of astronomical solutions, we provide a constrained absolute astrochronology of the Aptian stage. The 405 kyr ($g_{\text{Venus}}-g_{\text{Jupiter}}$) eccentricity astronomical timescale indicates a minimal duration of ~9.4 Myr for the Aptian stage and an age of 122.6 ± 0.3 Ma for the base of the Aptian, consistent with radioisotope dating. We find a deviation in the periodicity of $g_{\text{Mercury}}-g_{\text{Jupiter}}$ eccentricity term in the mid-Aptian stage, at ca. 117.19 ± 0.3 Ma, that we ascribe as an expression of the resonance transition $\sigma = (g_{\text{Mercury}} - g_{\text{Jupiter}}) - (s_{\text{Mercury}} - s_{\text{Venus}})$, in relation with a strong chaotic orbital motion of Mercury. Such a geological observation is supported by a concomitant resonant transition in the La2004 astronomical model.

Keywords: Aptian; OAEs; astrochronology; Vocontian Basin; astronomical chaos; Mercury.

1. Introduction

During the Aptian stage of the Early Cretaceous epoch, from 113.2 to 121.4 million years ago (Gradstein et al., 2020), the Earth witnessed severe environmental perturbations under greenhouse conditions, which expressed in the sedimentary record as organic-rich clay, called black shales (e.g., Jenkyns, 2010). Black shales reflect profound changes to ocean circulation and chemistry, and document extraordinary enhanced nutrient availability, and dramatic decrease in dissolved oxygen concentrations in deep-sea environments leading to widespread ocean anoxia, known as Oceanic Anoxic Events (OAEs). The OAEs resulted in unusual organic productivity and accumulation of organic matter in ocean sediments as well as the formation of black shales, which are now the major petroleum source rocks in the world (Haq et al., 1987). The OAEs coincide with shifts in the carbon-isotope composition, which have been interpreted as global carbon cycle perturbation (e.g., Jenkyns, 2010). A succession of OAEs characterizes the Aptian stage; some of them register extreme global warmings along with biotic perturbations in calcareous nannoplankton and planktonic foraminifera (e.g., Leckie et al., 2002) in relation to increased atmospheric CO₂ concentration (Méhay et al., 2009; Naafs et al., 2016) and ocean acidification (Erba et al., 2010). These Aptian events may provide some analogues to the current global warming and anthropogenic ocean acidification (Erba et al., 2010; Stoll, 2016). Their study allows a better understanding of the consequent effects on the Earth's climate system under greenhouse conditions. Thus, the timing and duration of these events appear crucial to better understand their causal mechanisms.

Unfortunately, the duration of the Aptian stage is still widely debated (Gradstein et al., 2004, 2012, 2020; Huang et al., 2010), ranging approximately from 6.4 Myr to 13.42 Myr (Fiet, 2000; Huang et al., 2010; Gradstein et al., 2012, 2020; Leandro et al., 2022). These considerable differences resulted mainly from discrepancies between radiometric dating (Selby et al., 2009; Midtkandal et al., 2016; Olierlock et al., 2019; Gradstein et al., 2020; Zhang et al., 2021) and cyclostratigraphic-astrochronologic evaluation from Italian reference boreholes (Piobbico, Cismon, and Poggio le Guaine cores) in the Umbria Marche basin (Huang et al., 2010; Leandro et al., 2022).

Astrochronology is today a proven approach for geochronology (Hinnov, 2013; Gradstein et al., 2020) and for constraining astronomical modeling through, for example, the detection of chaotic transitions in the inner Solar System (Zeebe and Lourens, 2019). Detection of these chaotic transitions in the geological record provides valuable information for establishing reliable astronomical solutions over longer time intervals as astronomical models are subject to chaos in the deep geologic past (Laskar et al., 2004; Zeebe and Lourens, 2022).

Here we have undertaken a cyclostratigraphic study using high-resolution (5 cm) magnetic susceptibility (MS) variations of a 380 m thick Aptian record in the Tethyan Vocontian Basin of southeastern France, where OAEs are particularly well developed. The studied sections are characterized by a mean sedimentation rate about ten times higher than that of the Italian sections previously used to estimate the duration of the Aptian stage (350 m thick Aptian in Vocontian Basin vs. 32 and 34 m thick Aptian in Umbria Marche Basin) (Huang et al., 2010; Leandro et al., 2022). Using the stable 405 kyr ($g_{\text{Venus}}-g_{\text{Jupiter}}$) orbital eccentricity cycle (Laskar et al., 2004), which is exceptionally pronounced in the studied sections, combined with previously radiometric dating, we generate an absolute astronomical timescale (ATS) for the Aptian. Then, we provide precise estimates of the durations of the Aptian stage and OAEs. Finally, we use the generated ATS to explore the record of long-period orbital cyclicities for possible detection of the chaotic resonance transitions (Laskar et al., 2004; Westerhold et al., 2017; Ma et al., 2017; Zeebe and Lourens, 2019), which has never been investigated in the Aptian stage. We further explore correlations between the acquired cyclostratigraphic record and a set of astronomical solutions looking for potential similarities between the two.

2. Geologic and stratigraphic settings

2.1. Geological setting

During the Early Cretaceous, the Vocontian Basin (SE France) was located at a palaeolatitude of 25–30°N in the northwestern margin of the Tethyan Ocean (Masse et al., 2000). It was an area of hemipelagic sedimentation characterized by a palaeodepth of a few hundred meters (Wilpshaar et al., 1997). The Vocontian Basin is known for its fossiliferous strata of Early Cretaceous, including the historical stratotypes of several Cretaceous stages, comprising the Albian (e.g., The Albian GSSP is the studied Col de Pré-Guittard section). The abundant ammonite fauna provides key ages for the Sub-Mediterranean zonal standard for correlation. Deposition in the basin center was fairly continuous, and the relative contributions of carbonate and terrigenous clastics were modulated by the climate and sea-level changes on the surrounding margins. The pronounced Early Cretaceous alternations of clay and limestone in the Vocontian Basin were mainly governed by precession and eccentricity (Giraud et al., 1995; Boulila et al., 2008; Charbonnier et al., 2013).

2.2. Stratigraphic framework: Aptian reference composite succession

A total of seven well-dated sections covering successive time intervals were investigated (Figs. 1 and 2). These sections are Saut du Loup (upper Barremian), Angles (upper Barremian-lower Aptian), Combe Lambert (lower Aptian), Glaise (lower Aptian), Serre Chaitieu (lower Aptian), Beaudinard (lower-upper Aptian), and Col de Pré-Guittard (upper Aptian-lower Albian).

These well-known localities initially described by Bréhéret (1997), are frequently used to generate a composite lithostratigraphic section, covering the uppermost Barremian-uppermost Albian interval (Herrle and Mutterlose, 2003; Herrle et al., 2004; Bodin et al., 2015; Caillaud et al., 2022). Detailed lithological columns and magnetic susceptibility (MS) data of each section are provided in Figs. 1 and 2. The overlapping intervals of these individual sections are correlated using (i) the well-established ammonite biozonation (Bréhéret, 1997; Vermeulen, 2002; Herrle and Mutterlose, 2003; Herrle et al., 2004), (ii) the numerous basin-wide marker horizons, and (iii) the high-resolution MS variations (Figs. 1 and 2; *SI Appendix*, Fig. S1-S9). The Saut du Loup/Angles/Combe-Lambert/Glaise sections are well correlated using the biostratigraphical scheme of Vermeulen (2002), who developed an ammonite zonation from the *G. sartousiana* to the *D. deshayesi* Zones, and correlations are reinforced using the high-resolution MS variations (Fig. 1). The Glaise/Serre-Chaitieu/Beaudinard/Col-de-Pré-Guittard sections are correlated using high-resolution MS data anchored to the basin-wide marker horizons: the “*Niveau Blanc*”, a micritic carbonate bed; the “*Niveau Fallo*”, a series of organic rich layers (FA1-FA4; Bréhéret, 1997); and the “*Faisceau Fromage*”, which is characterized by an alternation of marly levels and limestone beds (Fig. 2).

The 380 m thick continuous composite record spanning the uppermost Barremian through the lowermost Albian interval in the Vocontian Basin is presented in Fig. 3. This latest Barremian-earliest Aptian lithological succession is composed of poorly bioturbated grey limestone alternating with dark-grey marlstone. The early Aptian-early Albian interval consists of a monotonous sequence of hemipelagic blue-grey marl succession (“*Marnes Bleues*” Formation), which is intercalated by marly limestones, limestones, bentonites, centimetric turbiditic layers, and by several laminated organic-rich intervals. These horizons represent the sedimentary hallmark of local to global events: the Goguel level (10-m thick interval, early Aptian), which corresponds to the regional lithological expression of Selli OAE1a (Westermann et al., 2013); the dark laminated horizons of the “*Niveau Noir*” (NN1-NN4); the organic-rich sediments of the “*Niveau Fallo*” (FA1 to FA4); and the Jacob and Kilian levels, which correspond to two of the four events of the OAE1b (late Aptian-early Albian), the two other events being out of the targeted time interval (Fig. 3).

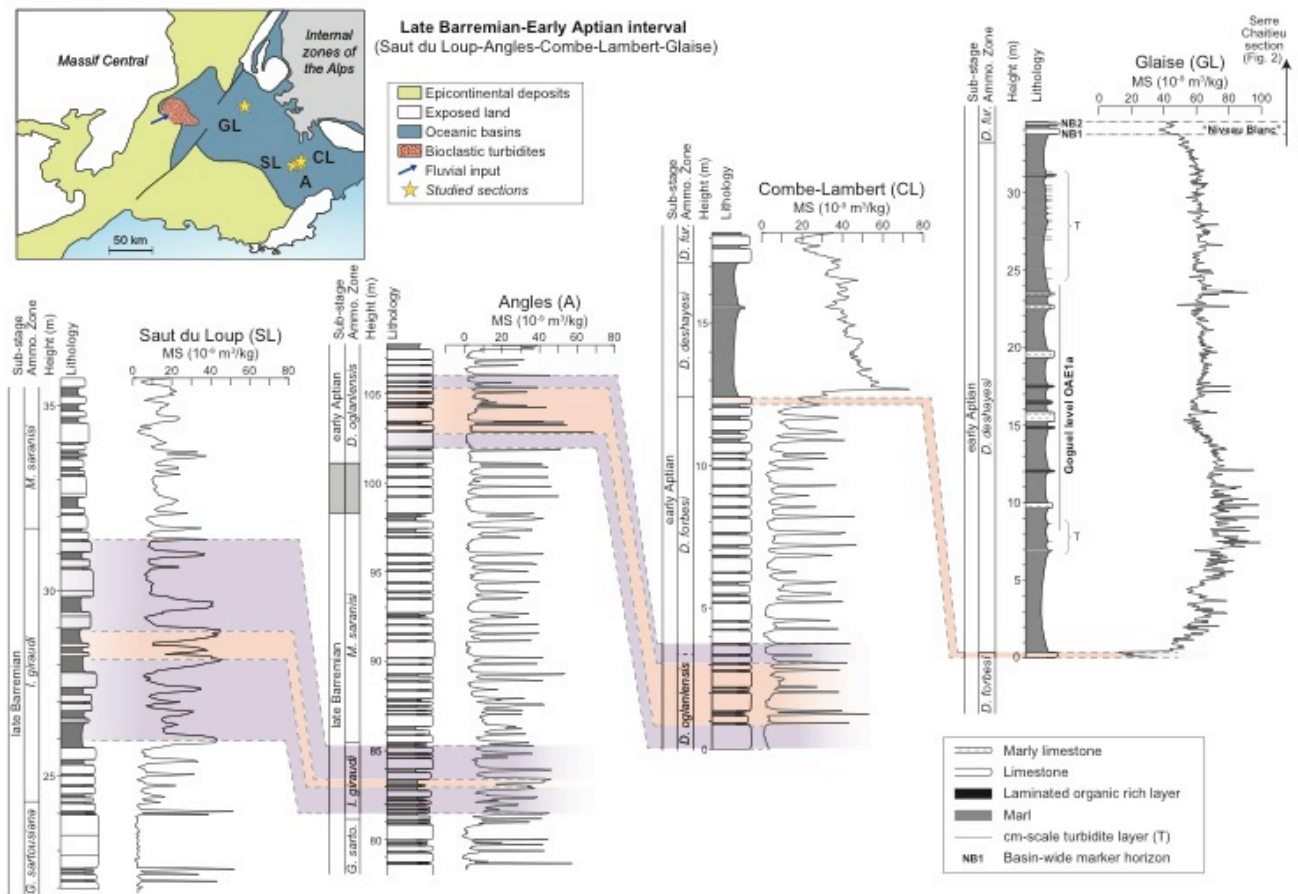


Fig. 1. Aptian paleogeographic map of the Vocontian Basin (modified after [Arnaud and Lemoine, 1993](#)), along with paleolocation of the studied sections. Biostratigraphy, lithology, and magnetic susceptibility (MS) data of the Saut du Loup, Angles, Combe Lambert, and Glaise sections. Dashed grey lines are correlations based on the well-established ammonite biozonation and basin-wide marker horizons, reinforced by the high-resolution MS variations. G. sarto.= G. sartousiana; D. fur.= D. furcata. Abbreviations for basin-wide stratigraphic markers, NB1 NB1 through NB2: “Niveau Blanc”.

3. Material and methods

3.1. Magnetic susceptibility (MS)

Each section was sampled with a regular sampling space of 5 cm (Figs. 1 and 2), thus a total of 8428 rock samples were collected. The magnetic susceptibility (MS) of each sample was measured using a Kappabridge MFK-1B (AGICO). The MS values were normalized to sample weight after correction from blanks and expressed in m^3/kg with a precision of $\pm 8 \times 10^{-10} \text{ m}^3/\text{kg}$. The highly resolved MS data capture the lithological variations (clay vs carbonate) even within the apparently homogeneous marly facies, i.e., with subtle changes in carbonate content (Fig. 3). There are several orders of MS values. The long-term irregular trends were measured and subtracted using the weighted average LOWESS method ([Cleveland, 1979](#)), implemented in *KaleidaGraph v. 4.1.3* software. Details on the detrending are provided in figure captions.

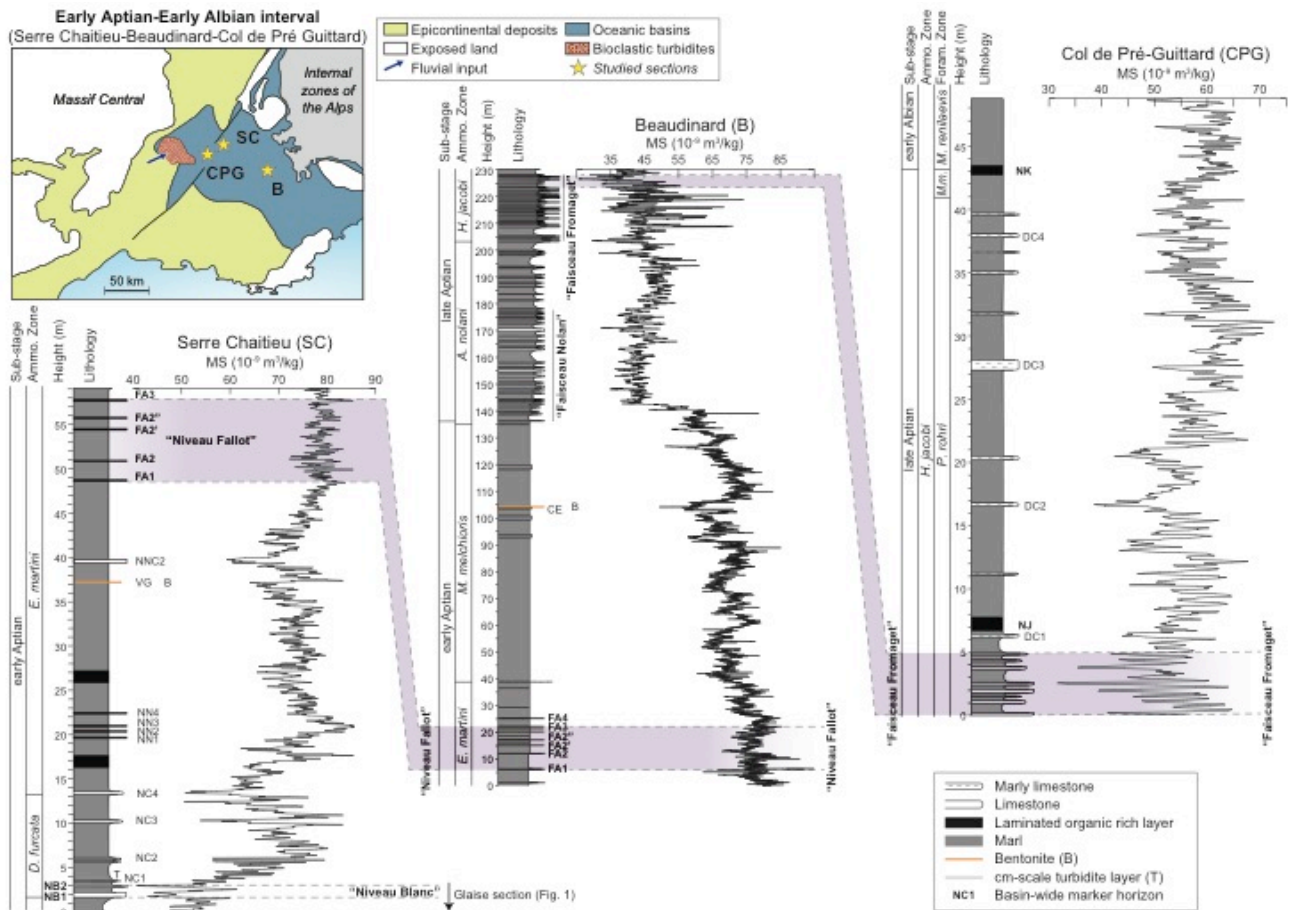


Fig. 2. Aptian paleogeographic map of the Vocontian Basin (modified after [Arnaud and Lemoine, 1993](#)), along with paleolocation of the studied sections. Biostratigraphy, lithology, and magnetic susceptibility (MS) data of the Serre Chaitieu, Beaudinard, and Col de Pré-Guittard sections. Dashed grey lines are correlations based on the well-established ammonite biozonation and basin-wide marker horizons, reinforced by the high-resolution MS variations. early Alb.= early Albian; M. m.= *M. miniglobularis*. Abbreviations for basin-wide stratigraphic markers, NB1 through NB2: “Niveau Blanc”, NC1 through NC4: “Niveau Calcaire”, NN1 through NN4: “Niveau Noir”, VG: Van Gogh bentonite, NNC2: “Niveau Noir Calcaire”, FA1 through FA4: “Niveau Fallot”, CE: Cézannes bentonite, DC1 through DC4: “Délit Calcaire”, NJ: “Niveau Jacob”, NK: “Niveau Kilian”.

3.2. Stable carbon isotopes ($\delta^{13}\text{C}_{\text{carb}}$)

The global OAE1a Selli interval was analyzed for carbon stable isotopes to characterize its structure in different segments and assess their respective durations. Bulk carbonate carbon stable isotope ratios ($\delta^{13}\text{C}$) were measured in 153 samples at the University of Lausanne, using a Thermo Fisher Scientific (Bremen, Germany) Gas Bench II carbonate preparation device connected to a Delta V Plus isotope ratio mass spectrometer. The $\delta^{13}\text{C}$ values are expressed in per mil relative to the Vienna PDB (V-PDB) standard. Precision of $\delta^{13}\text{C}$ measurements, estimated as the standard deviation of the mean calculated for replicate analyses of international standards NBS 18 ($\delta^{13}\text{C} = -5.04\text{‰}$), and NBS 19 ($\delta^{13}\text{C} = +1.95\text{‰}$), and the laboratory standard Carrara Marble ($\delta^{13}\text{C} = +2.05\text{‰}$), is $\pm 0.05\text{‰}$.

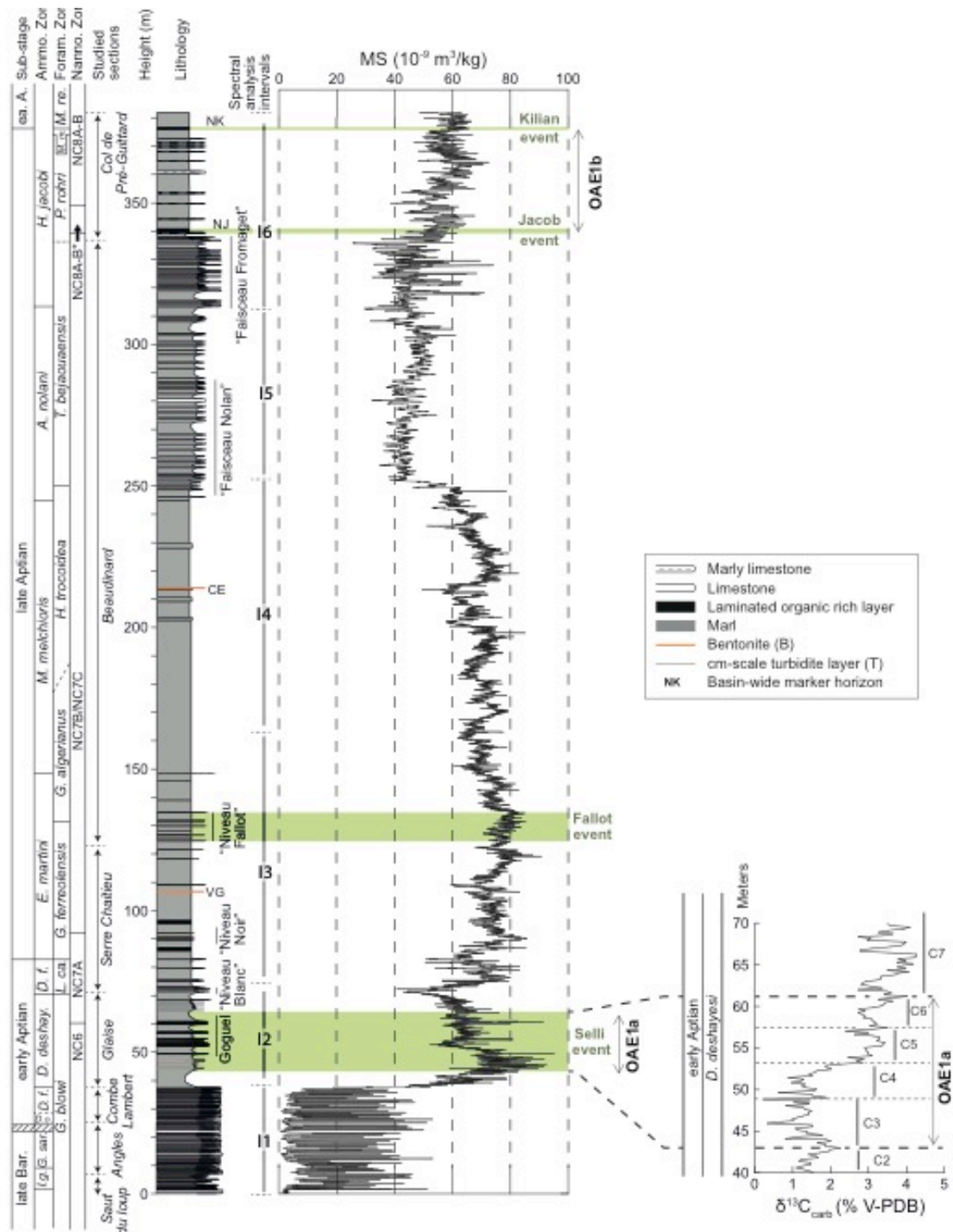


Fig. 3. Integrated biostratigraphic, lithostratigraphic, and magnetic susceptibility (MS) data of the uppermost Barremian through the lowermost Albian, along with basin-scale key stratigraphic markers, and OAEs intervals. The biostratigraphic framework of the composite section is given by ammonites, planktonic foraminifera, and calcareous nannofossils (Br  h  ret, 1997; Vermeulen, 2002; Herrle and Mutterlose, 2003; Herrle et al., 2003). Stratigraphic intervals recovered by the studied sections are indicated in the ‘studied sections’ column. The dark-grey bands indicate the position of the black-shale horizons recording the OAEs (OAE1a, Fallot, Jacob and Killian). Stratigraphic evolution of the $\delta^{13}\text{C}_{\text{carb}}$ record from the Glaise section. C3 to C6 indicate the position of the different segments characterizing the Early Aptian OAE1a interval (Menegatti et al., 1998). Late Bar. = late Barremian; I. g. = I. giraudi; G. sar. = G. sartousiana; D. o. = D. oglanlensis; D. f. = D. forbesi; D. desh. = D. deshaysi; D. f. = D. furcata; ea. A. = early Albian; L. ca. = L. cabri; M. m. = M. miniglobularis; M. re. = M. renilaevis; Ammo. Zone = Ammonite Zone; Foram. Zone = Foraminifera Zone; Nanno. Zone = Nannofossils Zone.

3.3. Time series analysis

For spectral analysis of MS data, we used the multitaper method (MTM, Thomson, 1982) associated with the robust red noise modelling as implemented in the SSA-MTM Toolkit (Ghil et al., 2002). Spectral analysis was applied per short intervals, jointly with a manual use of frequency ratio method (e.g., Huang et al., 1992; Mayer and Appel, 1999; Boulila et al., 2008) to recognize Milankovitch cycle bands, and assess potential changes in sedimentation rate. For the frequency-ratio method we used La2004 astronomical parameters (Laskar et al., 2004) centered on the Aptian-Albian boundary at nearly 113.2 Ma (Gradstein et al., 2020). Then, we used the automatic frequency ratio method, e.g. COCO: the correlation coefficient method, implemented in the *Acycle* v.2.0.8 freeware (Li et al., 2018) to statistically check the manual interpretation of Milankovitch cycle bands. For the extraction of the targeted cycles we used the Gaussian bandpass filter as implemented in the *AnalySeies* v.2.0.8 freeware (Paillard et al., 1996), as well as the Taner lowpass filtering in the *Acycle* v.2.4 freeware (Li et al., 2018). Finally, we tuned the MS record to the stable 405 kyr eccentricity cycle (Laskar et al., 2004) to orbitally calibrate the Aptian stage and the related ammonite zones. The tuning was performed using the *depth-to-time* Matlab routine (Li et al., 2018). We have tuned to a pure 405 kyr signal to establish a floating timescale (Laskar et al., 2004; Hinnov and Hilgen, 2012). Then, we anchored the 405 kyr floating timescale to the radiometrically dated age of the Aptian-Albian boundary at 113.2 Ma (Selby et al., 2009; Gradstein et al., 2020) for correlation with various astronomical models and versions of Earth's orbital eccentricity (Laskar et al., 2004, 2011).

4. Results

4.1. Magnetic susceptibility data

Magnetic susceptibility (MS) values range from 1.8 to $95.1 \times 10^{-9} \text{ m}^3/\text{kg}$ (Figs. 1 and 2). The limestones are characterized by low MS values due to diamagnetic minerals such as calcium carbonate, and the marls by moderate to higher values dependent on the concentration of the paramagnetic clays mineral they contain (Boulila et al., 2008). The evolution of MS values allows us to differentiate three intervals. In the lower interval from 0 to 37.5 m (*Imerites giraudi-Deshayesites forbesi* ammonite Zones) MS values are characterized by high frequency fluctuations of amplitudes ranging from 1.8 to $51.4 \times 10^{-9} \text{ m}^3/\text{kg}$, corresponding to rhythmical alternations of bioturbated white to grey limestones and grey to dark marls. In the middle interval from 37.5 to 250 m (*Deshayesites deshayesi-Parahoplites melchioris* ammonite zones) the MS values increase up to a maximum of $95.1 \times 10^{-9} \text{ m}^3/\text{kg}$. In this interval the high MS values, which evolves between 43.0 and $95.1 \times 10^{-9} \text{ m}^3/\text{kg}$, corresponds to the monotonous lithological succession of the hemipelagic blue-grey marl sediments interrupted by marly limestone beds and organic matter-rich horizons. Finally, in the upper clay-rich interval from 250 to 382.05 m (*Acanthohoplites nolani-Hypacauthoplites jacobi* Zones) the MS values increase from 25.7 to $73.0 \times 10^{-9} \text{ m}^3/\text{kg}$. Such a clay-rich sequence is frequently intercalated by rhythmic marl-limestone alternations (40 m: the “*Faisceau Nolan*” and 30 m: the “*Faisceau Fromage*”, Bréhéret, 1997), and by thick marly limestone beds (20-25 cm). Marl-limestone alternations can be subjected to diagenesis. However, there is increasing evidence for the astro-climatic control of these Vocontian Basin sediment records at different timescales and during various geological periods (Boulila et al., 2008, 2010, 2011; Charbonnier et al., 2013). Early diagenesis is very likely, but it would mimic or strengthen the primary astronomical signal in these alternating lithologies (Westphal, 2006; Boulila et al., 2011). This hypothesis is further argued on the basis of analyses of lithologically independent climatic proxies, such as clay mineralogy (e.g., Moiroud et al., 2012; Charbonnier et al., 2016; Corentin et al., 2020; Boulila et al., 2022).

The presence of smectite or irregular I-S R0 minerals, which appears very sensitive to high temperature linked to burial history (transformations at 60-70°C), in clay-rich sediment layers at

Angles, Combe Lambert, Serre Chaitieu, and Col de Pré-Guittard reveals that sedimentary series in the Vocontian Basin were not subjected to transformations by diagenetic burial (Godet et al., 2008; Ghirardi et al., 2014; Coarentin et al., 2020). The long-term trend in $\delta^{18}\text{O}_{\text{bel}}$ values throughout the latest Berriasian to the earliest Albian including our studied sections (Angles, Combe Lambert, Glaise, Serre Chaitieu, Beaudinard, and Col de Pré-Guittard) has been interpreted by Bodin et al. (2015) as being primarily driven by paleotemperature and $\delta^{18}\text{O}_{\text{seawater}}$ changes rather than due to a diagenetic overprint. Furthermore, we show here as also shown in previous studies that MS variations exhibit short- and long-term lithological (clay-carbonate) cycles matching Earth's orbital eccentricity modulation cycles (Charbonnier et al., 2013; Ghirardi et al., 2014; Martinez et al., 2015; Boulila et al., 2015).

4.2. Stable carbon isotopes data

The bulk carbonate $\delta^{13}\text{C}_{\text{carb}}$ values of the early Aptian OAE1a interval vary between 0.22 and 4.27‰ (Fig. 3). We use the terminology of Menegatti et al. (1998) to describe the carbon isotope stratigraphy. This $\delta^{13}\text{C}_{\text{carb}}$ record shows two negative excursions reaching minimal values of 0.33, and 0.22‰ at 45.95 and 48.85 m, respectively (segment C3). These two negative excursions are followed by a positive excursion up to 2.84‰ from 49.65 to 53.25 m (segment C4). From 53.25 to 57.45 m, the $\delta^{13}\text{C}_{\text{carb}}$ values fluctuates between 2.46 and 3.50‰ (segment C5). The top of the OAE1a interval is characterized by an increase from 2.73 to 4.02‰ between 57.45 and 61.2 m (segment C6). The $\delta^{13}\text{C}_{\text{carb}}$ pattern displays a similar structure, in shape and absolute values, to other reference sections from the Umbria Marche (Menegatti et al., 1998), Betic (Naafs et al., 2016), and South Provençal (Beil et al., 2020) Basins (Fig. 4).

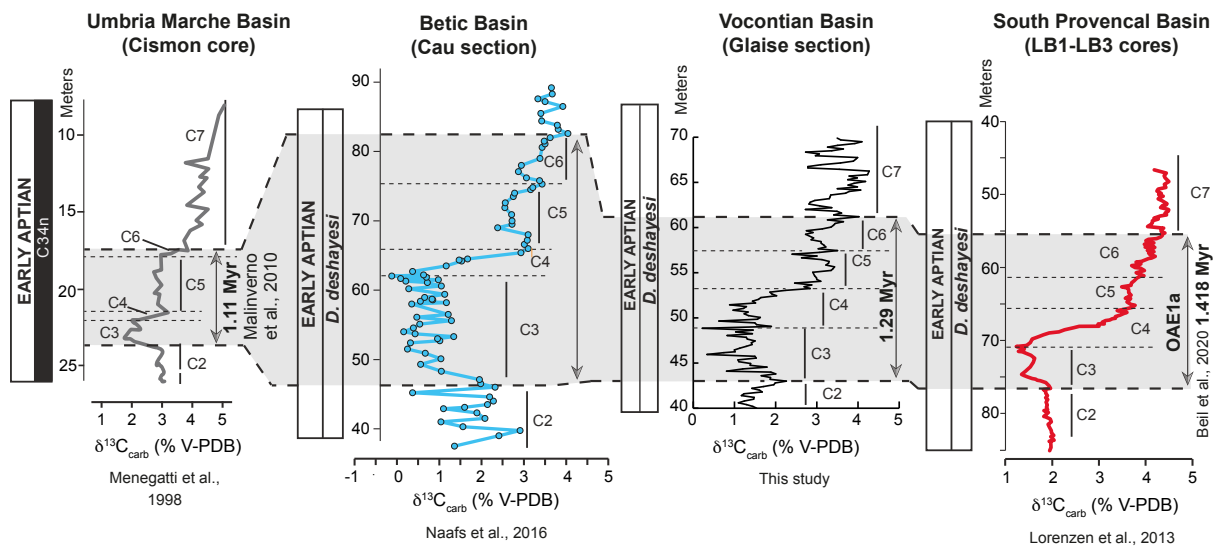


Fig. 4. Bulk carbonate isotope data and astronomical calibration of the OAE1a in the Vocontian Basin (This study), and comparison with previous studies in the Umbria Marche Basin (Menegatti et al., 1998), the Betic Basin (Naafs et al., 2016), and the South Provençal Basin (Lorenzen et al., 2013; Beil et al., 2020). OAE1a is defined as the interval covering segments C3-C6 (Menegatti et al., 1998).

4.3. Spectral analysis and astronomical calibration

Spectral analysis was first applied by short interval using visual inspection of MS variations, with a manual frequency ratio method to interpret sedimentary wavelengths as possible orbital frequencies and to assess potential changes in sedimentation rate. Thus, six distinct intervals have been identified throughout the record: I1 (0-39 m), I2 (34-75 m), I3 (69.4-163 m), I4 (155-260 m), I5 (250-315 m),

and I6 (310-382 m) (Fig. 3 and *SI Appendix*, Fig. S10). Each interval contains a prominent, significant low-frequency peak, of periods 10.87-m (I1), 5.85-m (I2), 13.16-m (I3), 23.2-m (I4), 26.3-m (I5), and 20-m (I6). The frequency ratio method and visual inspection of MS data in each interval indicate a common ratio of 1/4 (I1: 10.87/2.71 m; I2: 5.85/1.4 m; I3: 13.16/3.37 m; I4: 23.2/5.81 m; I5: 26.3/6.8 m; I6: 20/5m), matching the 405 kyr and the short eccentricity cyclicities respectively. Within each interval, frequency ratios also suggest that the ensemble of high-frequency peaks may correspond to the obliquity components (O1-O3, ratio 1/9, 1/12, and 1/14) and the precession components (P1 and P2 ratio 1/18 and 1/22.5) (*SI Appendix*, Figs. S11 and S12). Consequently, we interpreted the 10.87-m (I1), 5.85-m (I2), 13.16-m (I3), 23.2-m (I4), 26.3-m (I5), and the 20-m (I6) wavelengths as corresponding to the 405 kyr ($g_{\text{Venus}}-g_{\text{Jupiter}}$) eccentricity cycle. Additionally, we used the automatic frequency ratio method (e.g., COCO: the correlation coefficient method, Li et al., 2018) to statistically check the manual interpretation of Milankovitch cycle bands (Fig. 5 and Fig. S13). The statistical COCO tests by intervals reveal optimal sedimentation rates ranging from 1.8 to 7.2 cm/kyr (Fig. 5 and Fig. S13), which are very close to the visually inferred mean sedimentation rates (I1: 2.7 vs 3.2 cm/kyr; I2: 1.8 vs 1.4 cm/kyr; I3: 3.3 vs 3.2 cm/kyr; I4: 5.7 vs 5.5 cm/kyr; I5: 6.5 vs 7.2 cm/kyr; I6: 4.9 vs 4.5 cm/kyr). The above analyses are accomplished by the evolutive COCO (eCOCO), which tracks the evolution of optimal sedimentation rates along the composite section (Fig. 5 and Figs. S14 and S15). The eCOCO results strengthen single COCO outputs as well as our visual cyclostratigraphic interpretation.

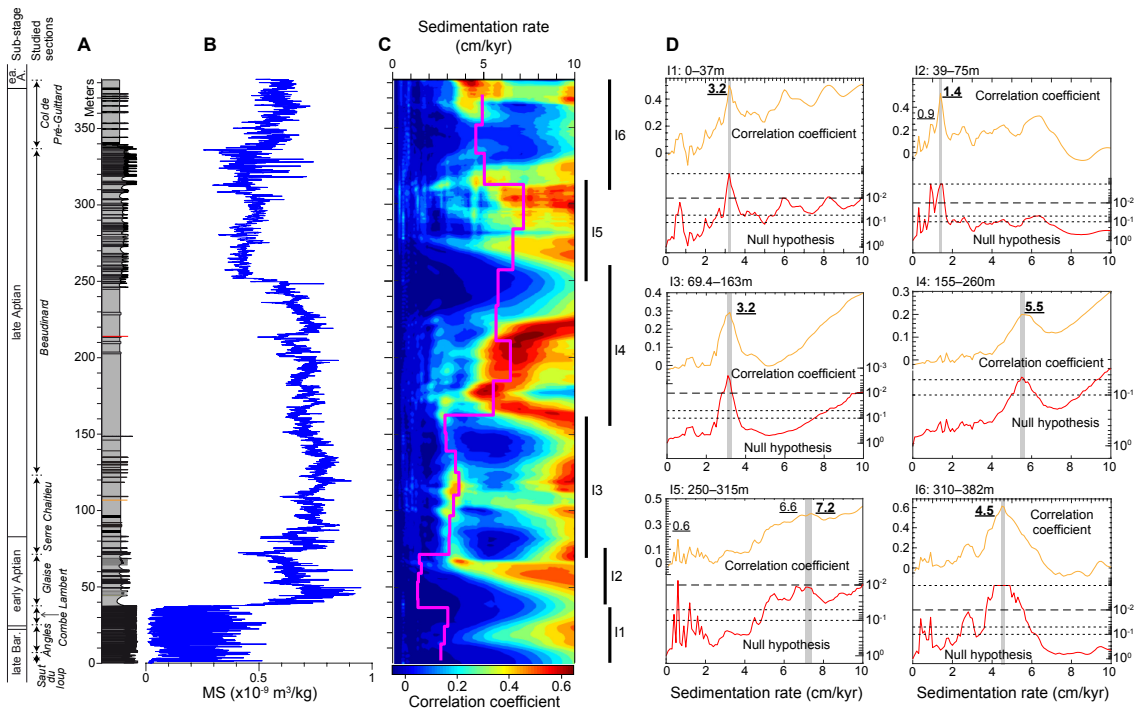


Fig. 5. Evolution of sedimentation rate in the studied Vocontian Basin section. (A) Lithostratigraphy along with the composite, raw MS data. (B) Pearson correlation coefficient of the evolutive eCOCO outputs (see Methods) applied to the 15% weighted average detrended MS data (see Fig. S14 for eCOCO applied to the raw MS data). The stair-like pink curve is the sedimentation rate inferred from the 405 kyr tuning of visually inspected sediment wavelengths related the 405 kyr eccentricity term. All eCOCO parameters and outputs are provided in Figs. S14 and S15. (C) Pearson correlation coefficient and Null hypothesis H0 for non-orbital forcing estimated by the COCO approach (see Methods), applied per individual intervals to test the optimal sedimentation rates of orbitally forced MS variations. Interval I1: Raw 0-37 m, Interval I2: 25% weighted average detrended 39-75 m, Interval I3: Raw 70-163 m, Interval I4: Raw 155-260 m, Interval I5: Raw 250-315 m, Interval I6: 45% weighted average detrended 310-382.05 m. All COCO parameters (inputs) and outputs are provided in Fig. S13.

One exception of statistically poor eCOCO result occurs at the transition from the marl-limestone alternations and the marly succession of the “*Marnes Bleues*” Formation of the lowermost Aptian, encoded by a strong shift in the MS signal (Fig. 5). However, single COCO outputs below and above the MS shift provide highly significant optimal sedimentation rates, again supported by our visual interpretation. Changes in sedimentation rate do not systematically depend on the studied, individual section. For instance, a significant change in sedimentation rate from ~3 cm/kyr to ~6 cm/kyr is recorded in the Beaudinard section within the lowermost part of *M. melchioris* ammonite zone (Fig. 5). In addition to the above mentioned MS shift at the alternating marl-limestone alternations (~3 cm/kyr mean sedimentation rate) and “*Marnes Bleues*” Formation (~1.5 cm/kyr mean sedimentation rate), we have noted an important increase in sedimentation rate (~1.5 cm/kyr to ~3 cm/kyr) at the Glaise/Serre Chaitieu section boundary. The two sections are well tied at the basin-wide “Niveau Blanc” lithostratigraphic marker (Br  h  ret, 1997). We infer this substantial change in sedimentation to lower sedimentation rates within the clay- and organic-rich OAE1a interval at Glaise, followed by higher sedimentation rates within the marly facies at Serre Chaitieu. Black shales have long been interpreted as recorders of phases of low sedimentation rates during periods of sea-level highs (Haq et al., 1987).

This 405 kyr metronome eccentricity component is prominent throughout the succession and was used to time-calibrate the section. A total of twenty-five 405 kyr eccentricity cycles are identified in the whole MS record, named Bar 1-Bar 2 for the Barremian stage and Apt 1 through Apt 23 for the Aptian stage (Fig. 6). This tuning results in a duration of 10.39 Myr for the studied interval, spanning the latest Barremian through the earliest Albian (Fig. 6). The spectrum of the tuned data shows significant frequencies close to theoretical astronomical periods (short eccentricity, obliquity, precession) (Laskar et al., 2004) (Fig. 7). The periodicities from 88.46 to 112.36 kyr may represent the short eccentricity (e), and the periodicities from 31.20 to 45.34 kyr may correspond to the obliquity components (O1, O3). The periodicities from 14.87 to 23.32 kyr are close to the precession components (P1, P2, P3) (Fig. 7). Additionally, the spectrum of the 405 kyr tuned series shows two prominent peaks at 1.13 and 0.946 Myr (Fig. 7), which may represent long-period eccentricity components (see Discussion).

5. Discussion

5.1. Duration of the Aptian stage

The Barremian-Aptian boundary (BAB) is defined at the base of the reverse magnetic polarity chron M0r (Gradstein et al., 2012). The first occurrence (FO) of *Deshayesites oglanlensis* ammonite is also used as a robust marker for the BAB in the Tethyan Realm (Reboulet et al., 2006). The latest Barremian interval is characterized by a global, negative peak in the $\delta^{13}\text{C}$ record, known as the Taxy event (Stein et al., 2011), which is close to the BAB and used as a regional chemostratigraphic marker among (hemi-) pelagic sections in the Vocontian, the South Provencal, and the Brian  onnais basins of France, and the Umbria Marche Basin in Italy (Godet et al., 2006; Stein et al., 2011). The BAB interval at the studied Angles section in the Vocontian Basin is marked by a drop-in abundance and diversity in ammonites (Vermeulen, 2002). At Angles it was tentatively placed between the minimum $\delta^{13}\text{C}$ values (latest Barremian) at bed 197 and the first appearance datum of the genus *Deshayesites* at bed 202 (Think Buble bed) (earliest Aptian) (Vermeulen, 2002; Godet et al., 2006). Finally, the Global Stratotype Section and Point (GSSP) for the base of the Albian stage has been placed at Col de Pr  -Guittard 40-cm above the base of the Kilian level with the FO of the planktonic foraminifera *Microhedbergella renilaevs* (Kennedy et al., 2017) (Fig. 6).

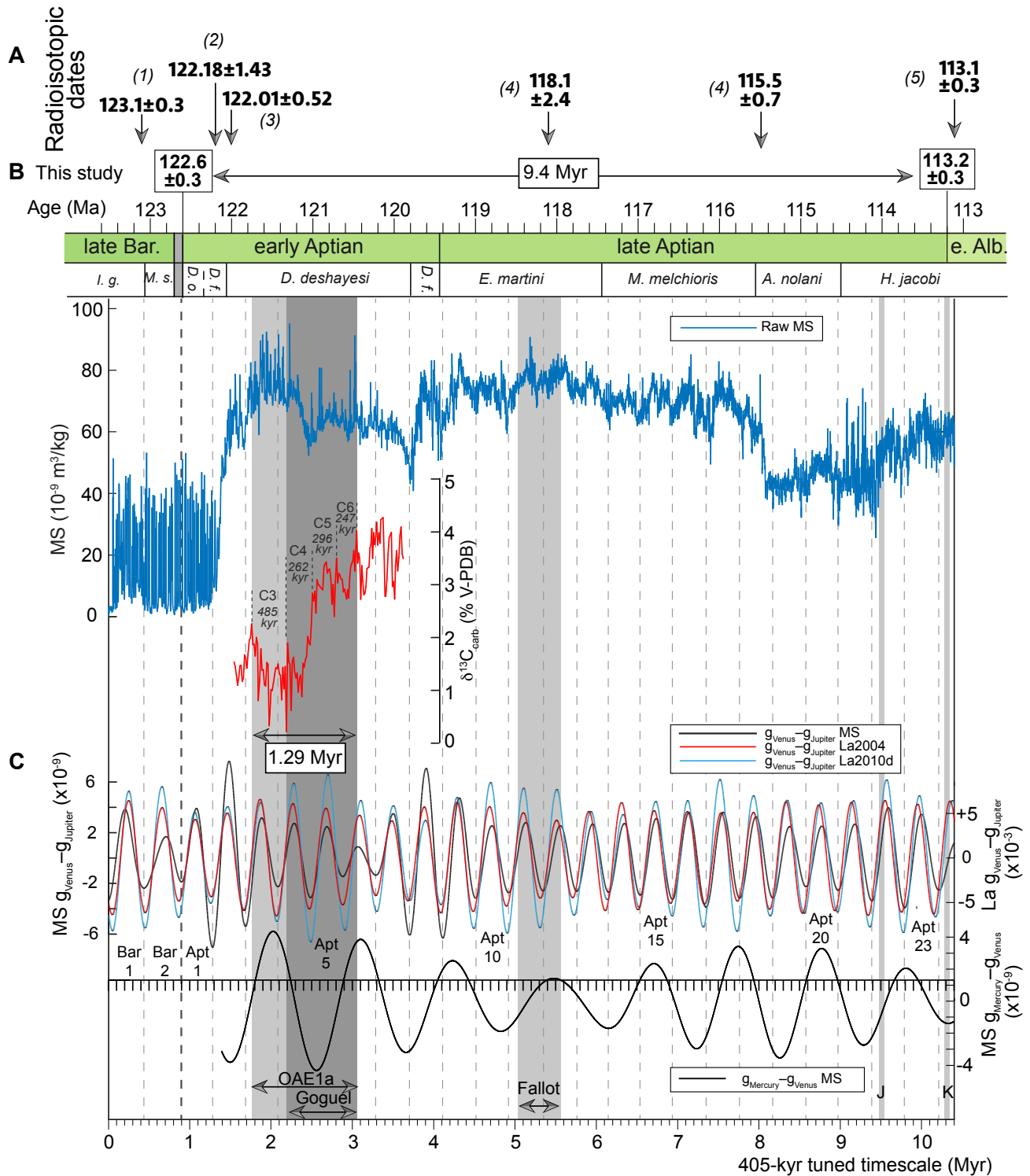


Fig. 6. Astronomical calibration of the Aptian stage and the associated OAEs. **(A)** Selected radioisotopic dates (in Ma) (1: Mitdkandal et al., 2016, 2: Pringle and Duncan, 1995, 3: He et al., 2008, 4: Gonzales Leon et al., 2008, 5: Selby et al., 2009), along with our estimation of ages and duration of the Aptian stage. The 405 kyr floating timescale in Panel ‘C’ is anchored at the age of the base of the Albian, at 113.2 ± 0.3 Ma, according to Gradstein et al. (2020), who refer to Selby et al. (2009). **(B)** The 405 kyr eccentricity tuned MS and $\delta^{13}\text{C}_{\text{carb}}$ data, along with recalibrated substages, isotopic segments, and the afferent ammonite zones. **(C)** Bandpass filters of the 405 kyr ($g_{\text{Venus}} - g_{\text{Jupiter}}$) and ~ 1 Myr ($g_{\text{Mercury}} - g_{\text{Jupiter}}$) eccentricity components in MS and astronomical data (0.0247 ± 0.001 and 0.092 ± 0.002 cycles/kyr, respectively). Bar1 through Apt23 are the interpreted 405 kyr eccentricity cycles. Vertical, grey-shaded bars indicate the position of the recovered OAEs.

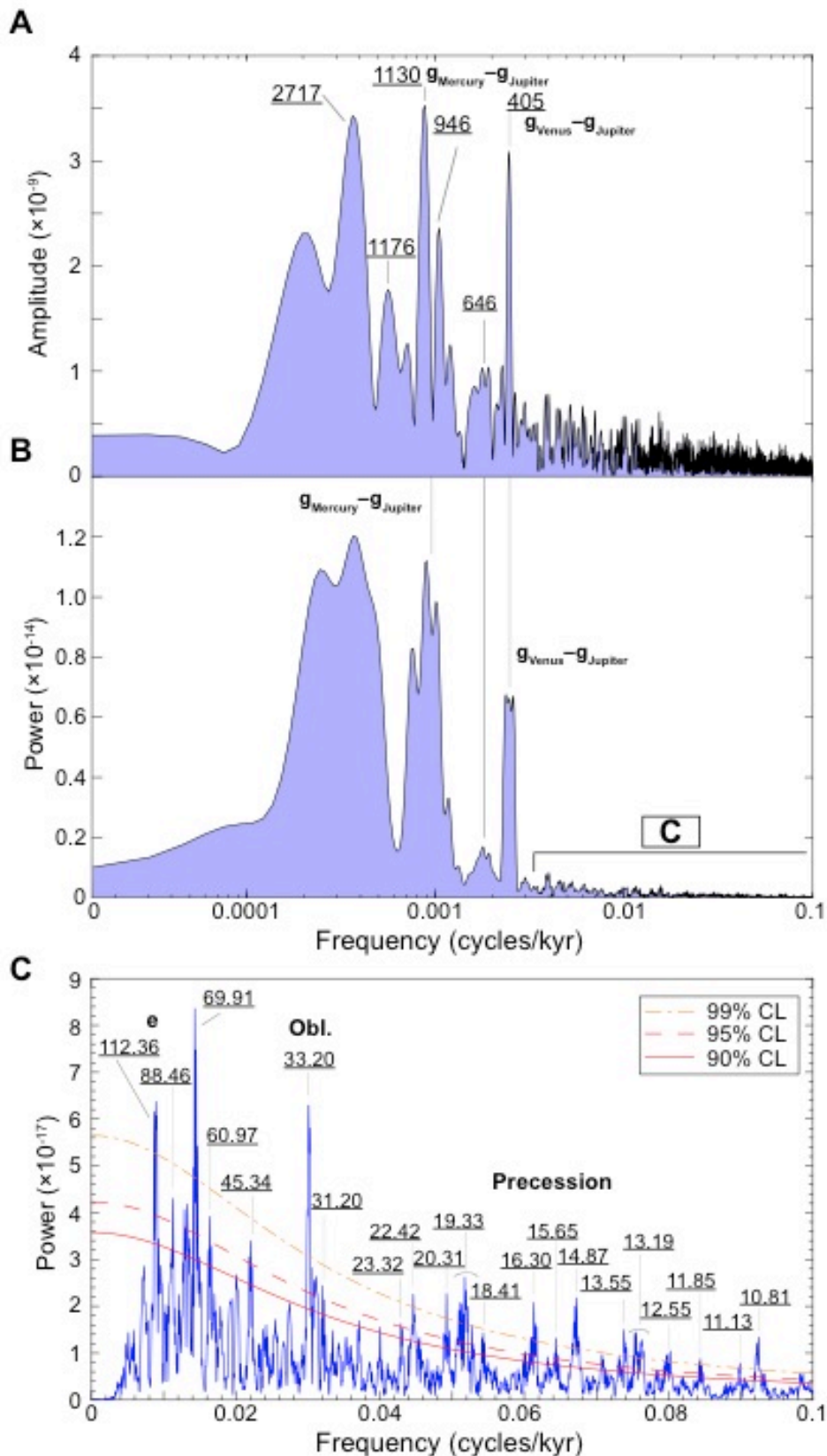


Fig. 7. Spectra of the detrended 405 kyr tuned MS series (with a 30% weighted average detrend) for the uppermost Barremian-lowermost Albian interval. **(A)** 2π -MTM amplitude spectrum of the tuned MS data. **(B)** 2π -MTM power spectrum of the tuned MS data. **(C)** Expanded view of the high-frequency portion of the 2π -MTM power spectrum shown in 'B' (low frequencies removed using the Taner lowpass filter, set at 0–1.8 cycles/Myr, and a roll-off of 10^{60}).

Using the 405 kyr orbital tuning of MS variations, we propose an Aptian stage duration, ranging from ~9.4 to 9.5 Myr (more than twenty-three 405 kyr eccentricity cycles, Apt1 through Apt23) (Fig. 6 and *SI Appendix*, Table S1). Our estimate differs from the $\sim 6.8 \pm 0.2$ Myr duration for the Aptian stage in the same Vocontian Basin (Fiet et al., 2006), the duration of $\sim 7.2 \pm 0.2$ Myr in shallow-marine carbonates in the southern Apennines (D’Argenio et al., 2004), and the durations of $\sim 6.4 \pm 0.2$ and $\sim 10.6 \pm 0.2$ Myr obtained from the pelagic Fucoïd Marls Formation in the Umbria Marche (Herbert et al., 1995; Fiet, 2000) (Table 1). However, these authors used only field lithologic and cyclostratigraphic interpretation of eccentricity cycles based on cycle counts, a limited methodology for accurate detection of all Milankovitch cycle bands. Our estimate is significantly shorter/longer than the ~ 13.42 and ~ 7.2 Myr durations deduced from spectral analyses of sediment data from the Piobbico/Cismon and the Poggio le Gaine cores in the Umbria Marche Basin, respectively (Huang et al., 2010; Leandro et al., 2022) (Table 1). This implies a difference of ~ 4 and ~ 2.2 Myr in the duration of the Aptian stage between our study and that of Huang et al. (2010) and Leandro et al. (2022) (Table 1). One hypothesis is that a ~ 4 Myr-long sedimentary gap occurred in the Vocontian Basin. A strong shift in the MS values is observed in the early Aptian at the transition between the bioturbated limestones alternating with marls, and dark-grey marly facies of the “*Marnes Bleues*” Formation (Fig. 3). This change in the lithology encoded in the MS signal, may reflect either combined effects of a change in the sedimentation regime accompanied by potential hiatuses or only a change in the sedimentation regime. We haven’t observed indications for possible hiatuses in the outcrops at this transition. The relatively good correspondence between our astronomical calibration of the Aptian stage and numerical calibration based on the radiochronologic approach (Section 5.1) excludes significant hiatuses in our record. Hiatuses at this lithological change may only be of thousands of years. Therefore, the impact of hypothetical hiatuses on our cyclostratigraphic results is minor, especially as we focus on the long-period orbital cycles (405 kyr and Myr-scale cyclicities).

Aptian stage

References	Basins	Sections/cores	Aptian stage
This study	Vocontian	composite section	9.4-9.5 Myr
Leandro et al., 2022	Umbria Marche	Poggio le Gaine core	7.1 Myr
Huang et al., 2010	Umbria Marche	Piobbico/Cismon core	13.42 Myr
Fiet et al., 2006	Vocontian	composite section	6.8 ± 0.2 Myr
Fiet, 2000	Umbria Marche	composite section	6.4 ± 0.2 Myr
D’Argenio et al., 2004	Carbonate platform Apennines	composite section	7.2 ± 0.2 Myr
Herbert et al., 1995	Umbria Marche	Piobbico core-sections	10.6 Myr

OAE1a

References	Basins	Sections/cores	C3	C4	C5	C6	OAE1a (C3-C6 segments)
This study	Vocontian	composite section	485 kyr	262 kyr	296 kyr	247 kyr	1.29 Myr
Beil et al., 2019	South Provencal	LB1-LB3 cores	434 kyr	388 kyr	281 kyr	315 kyr	1.418 Myr
Leandro et al., 2022	Umbria Marche	Poggio le Gaine core					0.920 Myr
Malinverno et al., 2010	Umbria Marche	Cismon APTICORE	46.7 kyr	239 kyr	510 kyr	349 kyr	1.11 ± 0.11 Myr
Li et al., 2008	Carbonate platform Mexico	Santa Rosa Canyon	44 kyr	930 kyr		310 kyr	1.28 Myr
	North Atlantic Ocean	DSDP Site 398		1-1.2 Myr			1-1.2 Myr
	Umbria Marche	Cismon APTICORE	27-41 kyr	330 kyr	570 kyr	330 kyr	1.27 Myr

Fallot, Jacob, and Kilian events

References	Basins	Sections/cores	Fallot event	Jacob event	Kilian event
This study	Vocontian	composite section	0.4865 Myr	25 kyr	32 kyr
Leandro et al., 2022	Umbria Marche	Poggio le Gaine core	0.15 Myr	30 kyr	90 kyr
Huang et al., 2010	Umbria Marche	Piobbico/Cismon core	0.360 Myr	40 kyr	120 kyr

Table 1. Comparison of durations of the Aptian stage and the OAEs in the Vocontian Basin (Fiet et al., 2006 and this study), the Umbria Marche Basin (Herbert et al., 1995; Fiet, 2000; Li et al., 2008; Huang et al., 2010; Malinverno et al., 2010; Leandro et al., 2022), the carbonate platform Apennines (D’Argenio et al., 2004), the North Atlantic Ocean (Li et al., 2008), in Mexico (Li et al., 2008), and the South Provencal Basin (Beil et al., 2020).

The Vocontian reference successions appear relatively complete with regard to the ammonite and planktonic foraminifera biozonations (Br  h  ret, 1997; Vermeulen, 2002; Herrle and Mutterlose, 2003; Herrle et al., 2003). The carbon isotope stratigraphy of the Vocontian basin is proposed by Herrle et al. (2004) as the standard reference curve for the Aptian to the Lower Albian due to the relative completeness and high temporal resolution of the stratigraphic succession. Additionally, our detailed field observations did not show any sedimentological indication of potential important hiatuses (e.g., slumps, erosional surfaces, hard grounds, condensation, mineral-fossil accumulations). The ~13.42 Myr duration of the Aptian stage (Huang et al., 2010) has also been discarded in the most recent geologic timescale GTS2020 (Gradstein et al., 2020). The difference between our study and the recent cyclostratigraphic approach in the Umbria-Marche Basin may be partly related to discrepancies in the durations of the Aptian events among the two basins. In the Vocontian Basin, the OAE1a is assessed at 1.29 Myr, while in the Umbria Marche Basin is estimated at 0.920 Myr (Table 1). Also, the Fallot event is estimated as 0.487 Myr in the Vocontian Basin, and as only 0.150 Myr in the Umbria-Marche Basin (Table 1). Additionally, a correlation between the two cyclostratigraphic signals in the Vocontian and Umbria-Marche basins indicates that the interval from the top of the Fallot event to the base of the Jacob level includes six 405 kyr eccentricity cycles (~2.4 Myr) in the Umbria-Marche Basin (Leandro et al., 2022) compared to more than nine and a half cycles (~3.911 Myr) in the Vocontian Basin (Fig. 6), implying a difference of ~1.5 Myr between the two basins. Thus, we suggest that the difference of ~2.2 Myr in the duration of the Aptian stage between the Vocontian and Umbria-Marche basins is likely due to condensations in the late Aptian within the OAE1a and Fallot events in the Umbria Marche Basin. This hypothesis is supported by comparing the Aptian mean sedimentation rate, which is extremely different between the two basins, 3.75 cm/kyr in the Vocontian Basin versus only 0.45 cm/kyr in the Umbria Marche Basin (Leandro et al., 2022).

Using the radiometric age of the base of the Albian at 113.2±0.3 Ma (Gradstein et al., 2020) well constrained by high-precision U-Pb dating (Selby et al., 2009) along with our astronomical calibration of the Aptian stage, the age of BAB can be assessed at 122.6 ±0.3 Ma (Fig. 6). This age is in good agreement with either the U-Pb 123.1±0.3 Ma date from drill-cores in Svalbard (Midtkandal et al., 2016; Zhang et al., 2021), or the recalibrated ⁴⁰Ar/³⁹Ar 122.01±0.52 Ma date from the Mashenmiao-Zhuanchengzi section (northeast China) (He et al., 2008). Our estimate also falls within the range of radio-isotopic dates compiled by Olierook et al. (2019), which indicate that the BAB age must be no older than 123.8 Ma and no younger than 121.8 Ma. Nevertheless, our interpretation, including uncertainties, implies a slightly older (300 kyr) BAB age than the 121.4±0.6 Ma age proposed by the latest GTS (Gradstein et al., 2020). In contrast, the extrapolated ages of 120.4±0.3 Ma and 126.62±0.3 Ma for the BAB based on the shorter (7.2 Myr, Leandro et al., 2022) or the longer (13.42 Myr, Huang et al., 2010) options for the Aptian duration are not compatible with radiometric ages. Consequently, we suggest that our revised cyclostratigraphic duration of the Aptian stage (9.4 Myr) as well as the potential age of BAB (122.6 ±0.3 Ma) can provide additional constraints to improve the Early Cretaceous timescale.

5.2. Astronomical calibration and pacing of the Aptian oceanic anoxic events

The stratigraphic sequence spanning the uppermost Barremian–lowermost Albian interval of the Vocontian Basin is characterized by the recurrence of short-lived episodes of marine anoxia referred to as the Selli OAE1a (early Aptian), the Fallot event (late Aptian), and the Jacob and Kilian sub-events of the OAE1b (latest Aptian) (Fig. 3).

To assess the stratigraphic extent of OAE1a, we use the carbon isotope profile divided into eight segments recording the Selli level or its time equivalent (Menegatti et al., 1998). OAE1a is defined as the interval covering segments C3-C6 (Fig. 3). Using the 405 kyr tuned MS series, we estimate a duration of ~1.29 Myr for the OAE1a interval (Fig. 4). This duration is slightly shorter than the

durations inferred from Piobbico core in the Umbria-Marche Basin, Italy (~1.4 Myr, [Huang et al., 2010](#)) and the LB1 and LB3 cores in the South Provencal Basin (~1.418 Myr, [Beil et al., 2020](#)) (Table 1). Our estimate is close to the durations inferred from DSDP Site 398 (North Atlantic Ocean), Cison APTICORE (Umbria-Marche Basin), and Santa Rosa (Mexico), ranging from ~1 to 1.3 Myr ([Li et al., 2008](#); [Malinverno et al., 2010](#)) (Table 1). This is in contradiction with the recent ~0.920 Myr estimate also inferred from the Poggio le Gaine core of the Umbria Marche Basin ([Leandro et al., 2022](#)) (Table 1).

The duration of the entire Fallot event, which is characterized by a succession of six organic-rich layers named FA1 through FA4 (FA1, FA2, FA2', FA2'', FA3, and FA4) ([Br  h  ret, 1997](#)), is estimated as ~486.5 kyr. This duration differs significantly from previous durations inferred from the Piobbico core (~360 kyr, [Huang et al., 2010](#)) and the Poggio le Gaine core (~150 kyr, [Leandro et al., 2022](#)) (Table 1). However, at Poggio le Gaine, only the organic-rich layer FA3 is observed, which suggests either the existence of a possible hiatus or that the FA3 layer is only the one to have a supra-regional extension.

The duration of the Jacob and Kilian events in the Vocontian Basin are assessed at ~25 kyr and ~32 kyr, respectively. However, these durations are shorter than estimates from the Poggio le Gaine core (~30 and ~90 kyr; [Leandro et al., 2022](#)) and the Piobbico core (~40 and ~120 kyr; [Huang et al., 2010](#)) (Table 1). These events are defined by the stratigraphic extension of the laminated organic-rich layers. The difference in durations observed between the Vocontian and the Umbria Marche Basins can be explained by difference in sea floor oxygenation history in time during black shale formation between pelagic (1000-1500 m Umbria-Marche Basin) and hemipelagic (~500 m Vocontian Basin) environment.

Anchored by radiometric ages, the correlated 405 kyr tuned MS time series to a set of astronomical solutions ([Laskar et al., 2004, 2011](#)) show that there is no match between eccentricity maxima and the onset of the global OAE1a, Fallot, Jacob, and the global Kilian events (Fig. 6). Furthermore, mercury (Hg) anomalies and osmium isotopes indicate that magmatic pulses related to the Greater Ontong Java and Kerguelen large igneous provinces occurred at the onset of the global OAE1a and Kilian events, respectively (e.g., [M  hay et al., 2009](#); [Charbonnier and F  llmi, 2017](#); [Matsumoto et al., 2020](#); [Bracquart et al., 2022](#)). The excess in volcanically released CO₂ may have amplified global warming and accelerated rates of Earth's system processes, including continental weathering and nutrient supply, anoxia, and biotic and carbon cycle perturbations ([Charbonnier and F  llmi, 2017](#)).

5.3. Aptian cyclostratigraphy detects a planetary chaotic transition

The orbits of planets in the Solar System are not stable (chaotic) at timescales of tens to hundreds of Myr ([Laskar, 1990, 1992](#); [Sussman and Wisdom, 1992](#)). As a result, collision between the inner planets at several Gyr is probable ([Laskar and Gastineau, 2009](#)). One prominent feature of the chaotic behavior in the Solar System is the presence of multiple secular resonances in the inner planet system ([Laskar, 1990, 1992](#); [Sussman and Wisdom, 1992](#)), with an exponential divergence that leads to an increase of the uncertainties in calculations by an order of magnitude every 10 Myr ([Laskar, 1989, 1990](#)). As a consequence, the precision of computations for some of Earth's orbital eccentricity cyclicities is limited in deep times, beyond ~50 Ma ([Laskar et al., 2004, 2011](#); [Zeebe and Lourens, 2019](#)). Dynamical secular resonances can explicitly be expressed as combinations of the fundamental orbital frequencies that we can detect in the sedimentary record, such as the secular resonance $\theta = 2$ ($g_{\text{Mars}} - g_{\text{Earth}} - (s_{\text{Mars}} - s_{\text{Earth}})$) that link Earth's and Mars' orbital secular frequencies (g_k for eccentricities and s_k for inclinations). This resonance includes two long-period orbital periodicities $g_{\text{Mars}} - g_{\text{Earth}}$ in the eccentricity, and $s_{\text{Mars}} - s_{\text{Earth}}$ in the obliquity, with their respective Cenozoic mean values of 2.4 and 1.2 Myr. These mean periods could deviate in deeper geological times, in the Mesozoic for example, due to the chaotic behavior of the orbital motion in the inner Solar System ([Laskar, 1989, 1990](#)). The 1.2 and 2.4 Myr orbital cycles have been detected with high fidelity in the

sedimentary archives (Boulila et al., 2011; Hinnov, 2013). Thus, geological records of these long-period orbital cyclicities in deep times can provide valuable information for astronomical modeling (Zeebe and Lourens, 2019, 2022) by the detection of timing of such resonant transitions (e.g., Boulila et al., 2014; Ma et al., 2017; Westerhold et al., 2017; Olsen et al., 2019; Zeebe and Lourens, 2019).

Few studies addressed this issue, focusing on the above mentioned secular resonance θ . Such investigation was mainly attempted by studying the behavior of the $g_{\text{Mars}}-g_{\text{Earth}}$ eccentricity term as macroscopic features in the variations of Earth's orbital eccentricity (e.g., Zeebe and Lourens, 2019). However, there is another secular resonance $\sigma = (g_{\text{Mercury}} - g_{\text{Jupiter}}) - (s_{\text{Venus}} - s_{\text{Mercury}})$ (Laskar, 1990), which has never been tested in cyclostratigraphy to possibly extract information about resonance transitions. The σ resonant argument is of equal importance to the θ argument because it includes the $g_{\text{Mercury}}-g_{\text{Jupiter}}$ eccentricity term, which can equally be detected in the sedimentary record (Abels et al., 2010; Boulila et al., 2021).

The 405 kyr tuned Aptian MS data show a macroscopic shift in the $g_{\text{Mercury}}-g_{\text{Jupiter}}$ frequency, occurring at ca. 117.19 Ma \pm 0.3 Ma (Fig. 8). The La2004 orbital solution (Laskar et al., 2004) shows a remarkable excursion in $g_{\text{Mercury}}-g_{\text{Jupiter}}$ eccentricity term, which started at around \sim 141.8 Ma, culminated at \sim 117.2 Ma and ended at \sim 109.8 Ma. The timing of the theoretical $g_{\text{Mercury}}-g_{\text{Jupiter}}$ optimal excursion is close to the age of $g_{\text{Mercury}}-g_{\text{Jupiter}}$ deviation observed in the Aptian strata. Interestingly, both astronomical and geological data show relatively longer and shorter values of the mean of $1/g_{\text{Mercury}}-g_{\text{Jupiter}}$ period (\sim 1.10 vs \sim 1.06 Myr respectively) when crossing the optimum of the mid-Aptian orbital excursion (Fig. 9). In the La2004 model there is a coexistent shift in $g_{\text{Venus}}-g_{\text{Mercury}}$ eccentricity term, but towards higher frequencies. While the perturbation in $g_{\text{Mercury}}-g_{\text{Jupiter}}$ has been ascribed as a possible consequence of the chaos expressed in the σ argument, the $g_{\text{Venus}}-g_{\text{Mercury}}$ term has been ascribed neither in θ nor in σ arguments. However, a recent study identified another important resonant term called $\sigma' = (g_{\text{Mercury}} - g_{\text{Venus}}) + (s_{\text{Mercury}} - s_{\text{Venus}})$ (Lithwick and Wu, 2011). Thus, deviation in $g_{\text{Venus}}-g_{\text{Mercury}}$ term is likely related to σ' .

The $g_{\text{Mars}}-g_{\text{Earth}}$ eccentricity term in the La2004 orbital model shows a concomitant mid-Aptian deviation towards higher frequencies, further supporting a perturbation reflected in both θ and σ arguments. Unfortunately, the $g_{\text{Mars}}-g_{\text{Earth}}$ period is not recorded in the Aptian sedimentary record; hence it cannot be tested for the chaos. It is important to note that during a chaotic transition, the affected eccentricity periodicities do not evolve in a similar way. For instance, $g_{\text{Venus}}-g_{\text{Mercury}}$ and $g_{\text{Mars}}-g_{\text{Earth}}$ have the same evolution towards higher frequencies, while $g_{\text{Mercury}}-g_{\text{Jupiter}}$ has an opposite evolution towards lower frequencies (Fig. 6). Also, $g_{\text{Mercury}}-g_{\text{Jupiter}}$ and $g_{\text{Venus}}-g_{\text{Mercury}}$ have a contrasting pattern, likely related to Mercury (g_1), a planet subjected to strong influence from the chaos (Laskar and Gastineau, 2009; Lithwick and Wu, 2011). Lithwick and Wu (2011) demonstrated that Mercury is perched at the threshold of chaos. In particular, they showed that an increase in eccentricities and inclinations of the planets by only 20% leads to violent instability, with Mercury ejected in \sim 100 Myr. The opposite pattern of long-term evolution in $g_{\text{Mercury}}-g_{\text{Jupiter}}$ and $g_{\text{Venus}}-g_{\text{Mercury}}$ originates from the fact that these two frequencies are related to (or modulated by) the libration frequency σ (Fig. 9). All this means that σ and σ' have the same libration frequency.

We have further checked the resonance argument σ by looking for a deviation in La2004 orbital inclination terms, particularly in the $s_{\text{Mercury}}-s_{\text{Venus}}$ term. We highlight a deviation in $s_{\text{Mercury}}-s_{\text{Venus}}$ orbital term, which is synchronous to $g_{\text{Mercury}}-g_{\text{Jupiter}}$ deviation. This result further reinforces that the 117 Ma optimal excursion in long-period eccentricity terms originates from the resonant term σ (*SI Appendix*, Fig. S16). From the analysis of La2004 model, we also show a potential coupling between the three resonant terms θ , σ , and σ' at this long chaotic excursion, centered on around 117 Ma (*SI Appendix*, Fig. S16).

We conclude that our cyclostratigraphic record confirms the reliability of the La2004 astronomical model for longer geologic time intervals, at least over the past 120 Ma, as attested by geological observation of the timing of the mid-Aptian resonance transition (optimum at around 117 Ma). Previous studies (Boulila et al., 2012) pointed to the reliability of La2004 orbital model

compared to other more recent astronomical models (Laskar et al., 2011) (*SI Appendix*, Fig. S17-S20). In particular, it has been shown that the La2004 model captures well long-period orbital cycles recovered in the geological record (Boulila et al., 2012, 2021; Ma et al., 2017).

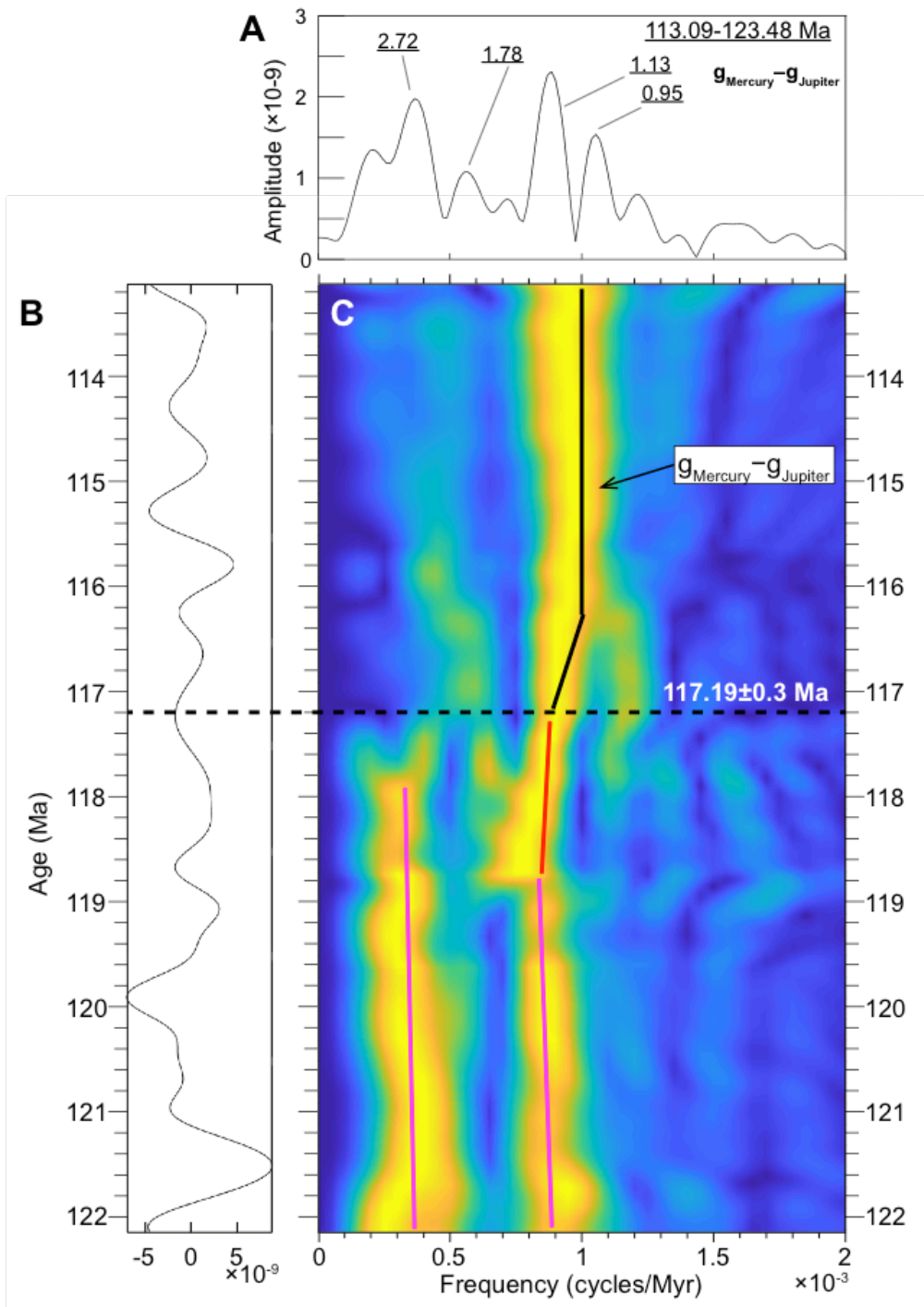


Fig. 8. Time-series analysis of low-frequency variations in Earth's orbital eccentricity of the MS data from the Vocontian Basin (SE France). **(A)** Amplitude spectrum of the tuned MS data. **(B)** Taner lowpass filter of MS data (0–1.8 cycles/Myr, Taner filter roll off at 10^{20}). **(C)** Evolutive FFT spectrogram of the lowpass filtered MS data (window = 10 Myr, step = 0.05 Myr). Note the strong shift at ~ 117.19 Ma in $g_{\text{Mercury}} - g_{\text{Jupiter}}$ eccentricity term. Vertical-bar color codes: blue then red, before the excursion or before the chaotic transition, black: after the chaotic transition.

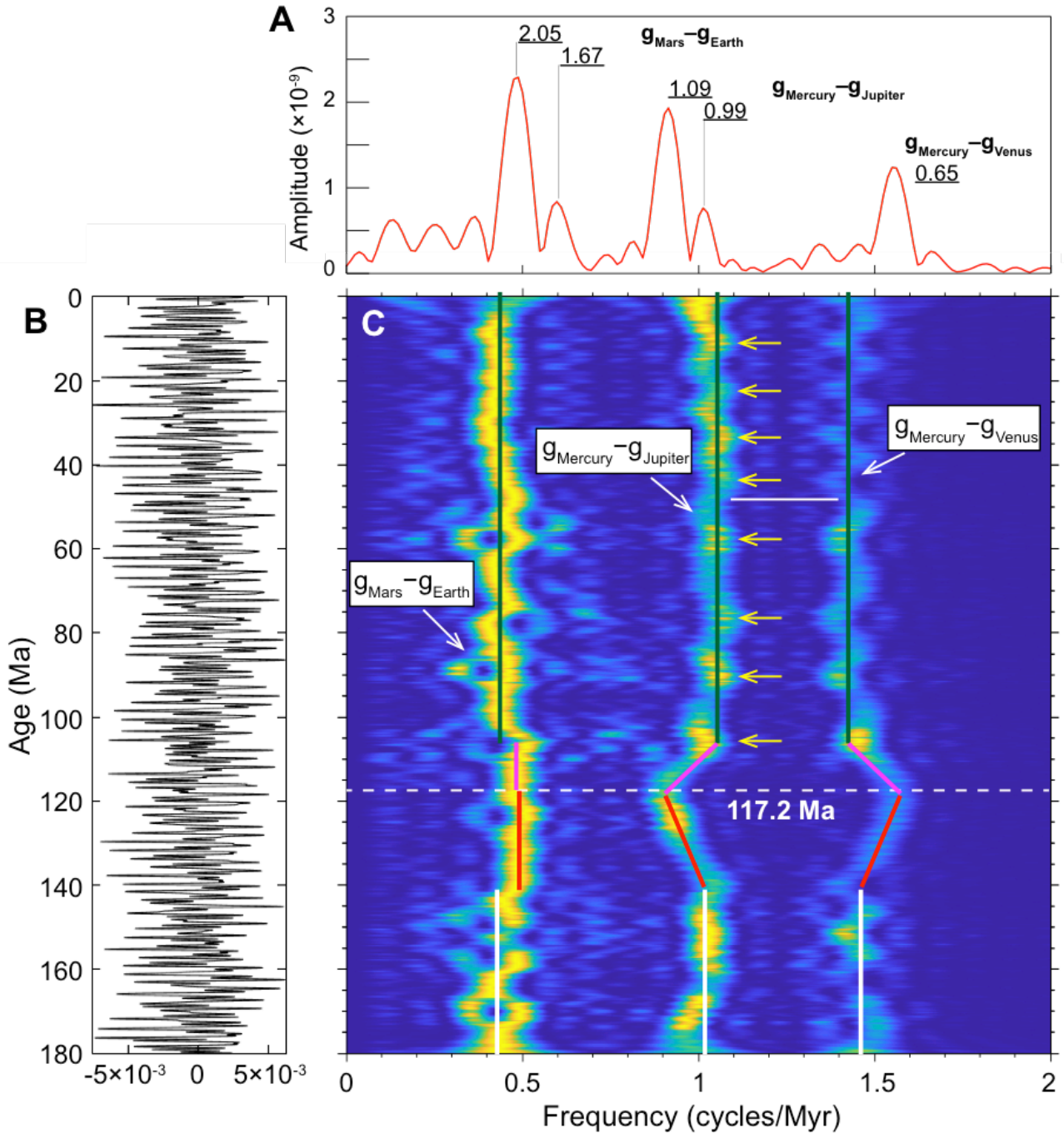


Fig. 9. Time-series analysis of low-frequency variations in Earth's orbital eccentricity of the La2004 astronomical model (Laskar et al., 2004). (A) Amplitude spectra of the astronomical model. (B) Taner lowpass filter of La2004 eccentricity (0–1.8 cycles/Myr, Taner filter roll-off at 10^{20}). (C) Evolutive FFT spectrogram of the lowpass filtered eccentricity (window = 10 Myr, step = 0.05 Myr). Note the strong shift at ~ 117.2 Ma in both $g_{\text{Mercury}} - g_{\text{Jupiter}}$ and $g_{\text{Mercury}} - g_{\text{Venus}}$ eccentricity terms. Vertical-bar color codes: white, before the excursion or before the chaotic transition, red then magenta: increasing/decreasing parts of the excursion, green: after the chaotic transition. Note that the values before and after the excursion (old and new stable states, respectively) are different. Horizontal solid, white line between horizontal, yellow arrows indicate timing of the change in the libration frequency σ from ~ 15 Myr to ~ 11 Myr (space between yellow arrows) at around 43 Ma, which corresponds to the age of the youngest resonance transition σ . The σ libration frequency modulates both $g_{\text{Mercury}} - g_{\text{Jupiter}}$ and $g_{\text{Mercury}} - g_{\text{Venus}}$. This result has been checked in another astronomical model.

6. Conclusions

An integrated stratigraphic and cyclostratigraphic approach was performed on the sedimentary sections in reference Vocontian Basin (SE France) outcrops spanning the uppermost Barremian-lowermost Albian interval. The obtained 10.4-Myr-long MS record allowed the following results:

- The 405 kyr eccentricity astronomical timescale indicates a minimal duration of ~ 9.4 Myr for the Aptian stage and therefore an age of 122.6 ± 0.3 Ma for the base of the Aptian.
- Our revised cyclostratigraphic duration of the Aptian stage appears concordant with numerical calibration based on the radiochronologic approach, which provide a new constraint on the Early Cretaceous timescale.
- Absolute astrochronology of the Aptian stage provide new constraint about the timing and the duration of the short-lived episodes of marine anoxia referred to as the Selli OAE1a (early Aptian), the Fallot event (late Aptian), and the Jacob and Kilian sub-events of the OAE1b (latest Aptian).
- The tuned MS data show a macroscopic shift in the periodicity of $g_{\text{Mercury}} - g_{\text{Jupiter}}$ eccentricity term in the mid-Aptian stage, at ca. 117.19 ± 0.3 Ma, that we ascribe as an expression of the resonance transition $\sigma = (g_{\text{Mercury}} - g_{\text{Jupiter}}) - (s_{\text{Mercury}} - s_{\text{Venus}})$, in relation with a strong chaotic orbital motion of Mercury. This interpretation is consistent with a resonant transition at the same time in the La2004 astronomical model.

Acknowledgements

G.C. has been supported by a grant of the French *Agence Nationale de la Recherche* (AstroMeso ANR-19-CE31-0002-01). This project has been supported by the French *Agence Nationale de la Recherche* and the European Research Council (ERC) under the European Union's Horizon 2020 research and innovation program (Advanced Grant AstroGeo-885250). We warmly thank Alexandre Lethiers for his substantial help in preparing most of the figures. We are grateful to Editor Prof. Laurence Coogan and the two anonymous reviewers for their constructive comments and useful suggestions.

References

- Abels, H.A., Abdul Aziz, H., Krijgsman, W., Smeets, S.J.B., Hilgen, F.J., 2010. Long-period eccentricity control on sedimentary sequences in the continental Madrid Basin (middle Miocene, Spain). *Earth and Planetary Sciences Letters* 289, 220–231.
- Arnaud, H., Lemoine, M., 1993. Structure and Mesozoic-Cenozoic evolution of the South-East France Basin (SFB). *Géol. Alpine, Série spéciale 'Colloques et Excursions'* 3, 3–58.
- Beil, S., Kuhnt, W., Holbourn, A., Scholz, F., Oxmann, J., Wallmann, K., Lorenzen, J., Aquit, M., Chellai, E.H., 2020. Cretaceous oceanic anoxic events prolonged by phosphorus cycle feedback. *Climate of the Past* 16, 757–782.
- Bodin, S., Meissner, P., Janssen, N.M.M., Steuber, T., Mutterlose, J., 2015. Large igneous provinces and organic carbon burial: Controls on global temperature and continental weathering during the Early Cretaceous. *Global and Planetary Change* 133, 238–253.
- Boulila, S., Charbonnier, G., Galbrun, B., Gardin, S., 2015. Climatic precession is the main driver of Early Cretaceous sedimentation in the Vocontian Basin (France): Evidence from the Valanginian Orpierre succession. *Sedimentary Geology* 324, 1–11.
- Boulila, S., de Rafélis, M., Hinnov, L.A., Gardin, S., Galbrun, B., Collin, P.-Y., 2010. Orbitally forced climate and sea-level changes in the Paleocene Tethyan domain (marl–limestone alternations, Lower Kimmeridgian, SE France). *Palaeogeography Palaeoclimatology Palaeoecology* 292, 57–70.
- Boulila S., Galbrun B., Gardin S., Pellenard P., 2022. A Jurassic record encodes an analogous Dansgaard–Oeschger climate periodicity. *Scientific Reports* 12:1968, DOI: 10.1038/s41598-022-05716-8.
- Boulila, S., Galbrun, G., Hinnov, L.A., Collin, P.Y., 2008. High-resolution cyclostratigraphic analysis from magnetic susceptibility in a Lower Kimmeridgian (Upper Jurassic) marl–limestone succession (La Méouge, Vocontian Basin, France). *Sedimentary Geology* 203, 54–63.
- Boulila, S., Galbrun, G., Huret, E., Hinnov, L.A., Rouget, I., Gardin, S., Bartolini, A., 2014. Astronomical calibration of the Toarcian Stage: Implications for sequence stratigraphy and duration of the early Toarcian OAE. *Earth and Planetary Science Letters* 386, 98–111.

- Boulila, S., Galbrun, B., Laskar, J., Pälike, H., 2012. A 9 myr cycle in Cenozoic $\delta^{13}\text{C}$ record and long-term orbital eccentricity modulation: Is there a link? *Earth and Planetary Science Letters* 317-318, 273–281.
- Boulila, S., Galbrun, B., Miller, K.G., Pekar, S.F., Browning, J.V., Laskar, J., Wright, J.D., 2011. On the origin of Cenozoic and Mesozoic “third-order” eustatic sequences. *Earth-Science Reviews* 109, 94-112.
- Boulila, S., Gardin, S., de Raféllis, M., Hinnov, L.A., Galbrun, B., Collin, P.Y., 2011. Reply to the Comment on “Orbitally forced climate and sea-level changes in the Paleocene Tethyan domain (marl-limestone alternations, Lower Kimmeridgian, SE France)” by S. Boulila et al. (2010). *Palaeogeography Palaeoclimatology Palaeoecology* 306, 252–257.
- Boulila, S., Haq, B.U., Hara, N., Müller, R.D., Galbrun, B., Charbonnier, G., 2021. Potential encoding of coupling between Milankovitch forcing and Earth’s interior processes in the Phanerozoic eustatic sea-level record. *Earth-Science Reviews* 220, 103727.
- Bracquart, E., Charbonnier, G., Garel, S., Munier, T., Adatte, T., Danzelle, J., 2022. New evidences of subareal volcanism as a trigger for the Kilian event (Aptian-Albian transition) and major climatic changes from offshore Morocco (DSDP Site 545). *Global and Planetary Change*. 218, 103959.
- Bréhéret, J.G., 1997. L’Aptien et l’Albien de la Fosse vocontienne (des bordures au bassin). Evolution de la sédimentation et enseignements sur les événements anoxiques. Société Géologique du Nord, Mémoire 25, 164 pp.
- Caillaud, A., Quijada, M., Hlohowskyj, S.R., Chappaz, A., Bout-Roumazeilles, V., Reynaud, J.Y., Riboulleau, A., Baudin, F., Adatte, T., Ferry, J.N., Tribovillard, N., 2022. Assessing controls on organic matter enrichments in hemipelagic marls of the Aptian-lower Albian Blue Marls of the Vocontian Basin (France): An unexpected variability observed from multiple organic-rich levels. *BSGF Earth Sciences Bulletin* 200051.
- Charbonnier, G., Boulila, S., Gardin, S., Duchamp-Alphonse, S., Adatte, T., Spangenberg, J.E., Föllmi, K.B., Colin, C., Galbrun, B., 2013. Astronomical calibration of the Valanginian “Weissert” episode: the Orpierre marl–limestone succession (Vocontian Basin, south- eastern France). *Cretaceous Research* 45, 25–42.
- Charbonnier, G., Duchamp-Alphonse, S., Adatte, T., Föllmi, K.B., Spangenberg, J.E., Gardin, S., Galbrun, B., Colin, C., 2016. Eccentricity paced monsoon-like system along the northwestern Tethyan margin during the Valanginian (Early Cretaceous): New insights from detrital and nutrient fluxes into the Vocontian Basin (SE France). *Palaeogeography, Palaeoclimatology, Palaeoecology* 443, 145-155.
- Charbonnier, G., Föllmi, K.B., 2017. Mercury enrichments in lower Aptian sediments support the link between Ontong Java large igneous province activity and oceanic anoxic episode 1a. *Geology* 1, 63–66.
- Cleveland, W.S., 1979. Robust locally weighted regression and smoothing scatterplots. *J. Am. Stat. Assoc.* 74, 829–836.
- Corentin, P., Deconinck, J.F., Pellenard, P., Amédéo, F., Bruneau, L., Chenot, E., Matrimon, B., Huret, E., Landrein, P., 2020. Environmental and climatic controls of the clay mineralogy of Albian deposits in the Paris and Vocontian Basins (France). *Cretaceous Research* 108, 104342.
- D’Argenio, B., Ferreri, V., Weissert, H., Amodio, S., Buonocunto, F.P., Wissler, L., 2004. A multidisciplinary approach to global correlation and geochronology. The Cretaceous shallow-water carbonates of southern Apennines, Italy. *SEPM Special Publication* 1, 103–122.
- Erba, E., Bottini, C., Weissert, H.J., Keller, C.E., 2010. Calcareous nannoplankton response to surface-water acidification around Oceanic Anoxic Event 1a. *Science* 329, 428–432.
- Fiet, N., 2000. Temporal calibration of the Aptian stage and related sub-stages by a cyclostratigraphic approach applied to the pelagic successions of the Umbria-Marche basin (Central Italy). *Bulletin de la Société Géologique de France* 171, 103–113.
- Fiet, N., Quidelleur, X., Parize, O., Bulot, L.G., Gillot, P.Y., 2006. Lower Cretaceous stage durations combining radiometric data and orbital chronology: Towards a more stable relative time scale? *Earth and Planetary Science Letters* 246, 407–417.
- Ghil, M., Allen, R.M., Dettinger, M.D., Ide, K., Kondrashov, D., Mann, M.E., Robertson, A., Saunders, A., Tian, Y., Varadi, F., Yiou, P., 2002. Advanced spectral methods for climatic time series. *Review Geophysics* 40, 1.1–1.41.
- Ghirardi, J., Deconinck, J.F., Pellenard, P., Martinez, M., Bruneau, L., Amiotte-Suchet, P., Pucéat, E., 2014. Multi-proxy orbital chronology in the aftermath of the Aptian Oceanic Anoxic Event 1a: Palaeoceanographic implications (Serre Chaitieu section, Vocontian Basin, SE France). *Newsletters on stratigraphy* 47, 247-262.
- Giraud, F., Beaufort, L., Cotillon, P., 1995. Periodicities of carbonate cycles in the Valanginian of the Vocontian Trough: a strong obliquity control. In: M.R. House, A.S. Gale, (Eds.), *Orbital Forcing Time Scales and Cyclostratigraphy*. Geological Society Special Publication 85, 143–164 (London).
- Godet, A., Bodin, S., Adatte, T., Föllmi, K.B., 2008. Platform-induced clay-mineral fractionation along a northern Tethyan basin-platform transect: implications for the interpretation of Early Cretaceous climate change (Late Hauterivian–Early Aptian). *Cretaceous Research* 29, 830-847.
- Godet, A., Bodin, S., Föllmi, K.B., Vermeulen, J., Gardin, S., Fiet, N., Adatte, T., Berner, Z., Stüben, D., Van de Schootbrugge, B., 2006. Evolution of the marine stable carbon- isotope record during the early Cretaceous: a focus on the late Hauterivian and Barremian in the Tethyan realm. *Earth Planetary Science Letters*. 242, 254–271.

- Gonzalez-Leon, C.M., Scott, R.W., Löser, H., Lawton, T.F., Robert, E., Valencia, V.A., 2008. Upper Aptian-Lower Albian mural formation: Stratigraphy, biostratigraphy, and depositional cycles on the Sonoran shelf, northern Mexico. *Cretaceous Research* 29, 249–266.
- Gradstein, F.M., Ogg, J.G., Schmitz, M., Ogg, G., 2012. *The Geologic Time Scale 2012*, vols. 1 and 2. Elsevier, 1444 p.
- Gradstein, F.M., Ogg, J.G., Smith, A., 2004. *Geological Time Scale*, Cambridge University Press.
- Gradstein, F.M., Ogg, J.G., Schmitz, M.D., Ogg, G.M., 2020. *The Geologic Time Scale 2020*, 2 volumes, 1390 pp. doi.org/10.1016/C2020-1-02369-3.
- Haq, B.U., Hardenbol, J., Vail, P.R., 1987. Chronology of fluctuating sea levels since the Triassic. *Science* 235, 1156–1167.
- He, H., Pan, Y., Tauxe, L., Qin, H., Zhu, R., 2008. Toward age determination of the M0r (Barremian-Aptian boundary) of the Early Cretaceous. *Physics of the Earth and Planetary Interiors* 169, 41–48.
- Herbert, T.D., Premoli Silva, I., Erba, E., Fischer, A.G., 1995. Orbital chronology of Cretaceous–Paleogene marine strata. *SEPM Special Publication* 54, 81–93.
- Herrle, J.O., Köbber, P., Friedrich, O., Erlenkeuser, H., Hemleben, C., 2004. High-resolution carbon isotope records of the Aptian to Lower Albian from SE France and the Mazagan Plateau (DSDP Site 545): a stratigraphic tool for paleoceanographic and paleobiologic reconstruction. *Earth and Planetary Science Letters* 218, 149–161.
- Herrle, J.O., Mutterlose, J., 2003. Calcareous nannofossils from the Aptian–early Albian of SE France: paleoecological and biostratigraphic implications. *Cretaceous Research* 24, 1–22.
- Herrle, J.O., Pross, J., Friedrich, O., Köbber, P., Hemleben, C., 2003. Forcing mechanisms for mid-Cretaceous black shale formation: evidence from the Upper Aptian and Lower Albian of the Vocontian Basin (SE France). *Palaeogeography, Palaeoclimatology, Palaeoecology* 190, 399–426. https://doi.org/10.1016/S0031-0182(02)00616-8.
- Hinnov, L.A., 2013. Cyclostratigraphy and its revolutionizing applications in the earth and planetary sciences. *GSA Bulletin* 125, 1703–1734.
- Hinnov L.A., Hilgen F.J. In: *The Geologic Time Scale 2012*. Gradstein F.M., Ogg J.G., Schmitz M., Ogg G.M., editors. Elsevier; Amsterdam: 2012. Cyclostratigraphy and astrochronology; pp. 63–83.
- Huang, Z., Boyd, R., O'Connell, S., 1992. Upper cretaceous cyclic sediments from hole 762C, exmouth plateau, northwest Australia. In: U. Von Rad, B.U. Haq, (Eds.), *Proc. Ocean Drilling Program*, 122. *Scientific Results* 259–277.
- Huang, C., Hinnov, L., Fischer, A.G., Grippo, A., Herbert, T., 2010. Astronomical tuning of the Aptian stage from Italian reference sections. *Geology* 38, 899–902.
- Jenkyns, H.C., 2010. Geochemistry of oceanic anoxic events: Review. *Geochemistry, Geophysics, Geosystems* 11, n/a–n/a. https://doi.org/10.1029/2009GC002788.
- Kennedy, J.W., Gale, A.G., Huber, B.T., Petrizzo, M.R., Bown, P., Jenkyns, H.C., 2017. The global boundary stratotype section and point (GSSP) for the base of the Albian stage, of the Cretaceous, the Col de Pré-Guittard section, Arnayon, Drôme, France. *Episodes* 40, 177–188.
- Laskar, J., 1989. A numerical experiment on the chaotic behaviour of the Solar System. *Nature* 338, 237–238.
- Laskar, J., 1990. The chaotic motion of the Solar System: a numerical estimate of the size of the chaotic zones. *Icarus* 88, 266–291.
- Laskar, J., 1992. La stabilité du Système Solaire, in *Chaos et Déterminisme*, A. Dahan et al., eds., Seuil, Paris.
- Laskar, J., Fienga, A., Gastineau, M., Manche, H., 2011. La2010: a new orbital solution for the long-term motion of the Earth. *Astronomy & Astrophysics* 532, A89. Doi:10.1051/0004-6361/201116836.
- Laskar, J., Gastineau, M., 2009. Existence of collisional trajectories of Mercury, Mars, and Venus with the Earth. *Nature* 459, 817–819.
- Laskar, J., Robutel, P., Joutel, F., Gastineau, M., Correia, A.C.M., Levrard, B., 2004. A long-term numerical solution for the insolation quantities of the Earth. *Astronomy & Astrophysics* 428, 261–285.
- Leandro, C.G., Savian, J.F., Kochhann, M.V.L., Franco, D.R., Coccioni, R., Frontalini, F., Gardin, S., Jovane, F., Figueiredo, M., Tedeschi, L.R., Janikian, L., Almeida, R.P., Trindade, R.I.F., 2022. Astronomical tuning of the Aptian stage and its implications for age recalibrations and paleoclimatic events. *Nature Communication* 13, :2941| https://doi.org/10.1038/s41467-022-30075-3.
- Leckie, R.M., Bralower, T.J., Cashman, R., 2002. Oceanic anoxic events and plankton evolution: Biotic response to tectonic forcing during the mid-Cretaceous. *Paleoceanography* 17, 1041, doi:10.1029/2001PA000623.
- Lorenzen, J., Kuhnt, W., Holbourne, A., Flögel, S., Moullade, M., Tronchetti, G., 2013. A new sediment core from the Bedoulian (Lower Aptian) stratotype at Roquefort-La Bédoule, SE France. *Cretaceous Research* 39, 6–16.
- Li, Y.X., Bralower, T.J., Montañez, I.P., Osleger, D.A., Arthur, M.A., Bice, D.M., Herbert, T.D., Erba, E., Silva, I.P., 2008. Toward an orbital chronology for the early Aptian oceanic anoxic event (OAE1a, ~120 Ma). *Earth Planetary Science Letters* 271, 88–100.
- Li, M., Kump, L.R., Hinnov, L.A., Mann, M.E., 2018. Tracking variable sedimentation rates and astronomical forcing in Phanerozoic paleoclimate proxy series with evolutionary correlation coefficients and hypothesis testing. *Earth Planetary Science Letters* 501, 165–179.

- Lithwick, Y., Wu, Y., 2011. Theory of secular chaos and Mercury's orbit. *Astrophys Journal* 739, 31.
- Ma, C., Meyers, S.R., Sageman, B.B., 2017. Theory of chaotic orbital variations confirmed by Cretaceous geological evidence. *Nature* 542, 468–479.
- Malinverno, A., Erba, E., Herbert, T.D., 2010. Orbital tuning as an inverse problem: Chronology of the early Aptian oceanic anoxic event 1a (Selli Level) in the Cismonte APTICORE, *Paleoceanography* 25, PA2203.
- Masse, J.P., Bouaziz, S., Amon, E.O., Baraboshin, E., Tarkowski, R.A., Bergerat, F., et al. 2000. Early Aptian (112–114 Ma), map 13. In: J. Dercourt, M. Gaetani, B. Vrielynck, E. Barrier, B. Biju-Duval, M.F. Brunet, J.P. Cadet, S. Crasquin, M. Sandulescu, eds. *Atlas Peri-Tethys: palaeoenvironmental maps, Explanatory notes*. Paris, 268 p.
- Matsumoto, H., Kuroda, J., Coccioni, R., Frontalini, F., Sakai, S., Ogawa, N.O., Ohkouchi, N., 2020. Marine Os isotopic evidence for multiple volcanic episodes during Cretaceous Oceanic Anoxic Event 1b. *Scientific Reports*. 10:12601, doi.org/10.1038/s41598-020-69505-x.
- Martinez, M., Deconinck, J.F., Pellenard, P., Riquier, L., Company, M., Reboulet, S., Moiroud, M., 2015. Astrochronology of the Valanginian-Hauterivian stages (Early Cretaceous): Chronological relationships between the Parana-Etendeka large igneous province and the Weissert and the Faraoni events. *Global and Planetary Change* 131, 158–173.
- Mayer, H., Appel, E., 1999. Milankovitch cyclicity and rock-magnetic signatures of paleoclimatic changes in the early Cretaceous biancone formation of the southern alps. Italy. *Cretaceous Research* 20, 189–214.
- Méhay, S., Keller, C.E., Bernasconi, S.M., Weissert, H., Erba, E., Bottini, C., Hochuli, P.A., 2009. A volcanic CO₂ pulse triggered the Cretaceous oceanic anoxic event 1a and a biocalcification crisis. *Geology* 37, 819–822.
- Menegatti, A.P., Weissert, H., Brown, R.S., Tyson, R.V., Farrimond, P., Strasser, A., Caron, M., 1998. High-resolution $\delta^{13}\text{C}$ -stratigraphy through the early Aptian “Livello Selli” of the Alpine Tethys. *Paleoceanography* 13, 530–545.
- Midtkandal, I., Svensen, H.H., Planke, S., Corfu, F., Polteau, S., Torsvik, T.H., Faleid, J.I., Grundvåg, S.A., Selnes, H., Kürschner, W., Olaussen, S., 2016. The Aptian (Early Cretaceous) oceanic anoxic event (OAE1a) in Svalbard, Barents Sea, and the absolute age of the Barremian-Aptian boundary. *Palaeogeography, Palaeoclimatology, Palaeoecology* 463, 126–135.
- Moiroud, M., Martinez, M., Deconinck, J.F., Monna, F., Pellenard, P., Riquier, L., Company, M., 2012. High-resolution clay mineralogy as a proxy for orbital tuning: Example of the Hauterivian-Barremian transition in the Betic Cordillera (SE Spain). *Sedimentary Geology* 282, 336–346.
- Naafs, B.D., Castro, J.M., De Gea, G.A., Quijano, M.L., Schmidt, D.N., Pancost, R.D., 2016. Gradual and sustained carbon dioxide release during Aptian Oceanic Anoxic Event 1a. *Nature Geoscience* 9, 135–139.
- Olierook, H.K.H., Jourdan, F., Merle, R.E., 2019. Age of the Barremian-Aptian boundary and onset of the Cretaceous Normal Superchron. *Earth- Science Reviews* 197, 102906.
- Olsen, P.E., Laskar, J., Kent, D.V., Kinney, S.T., Reynolds, D.J., Sha, J., Whiteside, J.H., 2019. Mapping Solar System chaos with the Geological orrery. *PNAS* doi/10.1073/pnas.1813901116.
- Paillard, D., Labeyrie, L., Yiou, P., 1996. Macintosh program performs timeseries analysis. *Eos* 77, 379.
- Pringle, M., Duncan, R., 1995. Radiometric ages of basement lavas recovered at Loen, Wodejebato, MIT, and Takuyo-Daisan Guyots, northwestern Pacific Ocean. *Proceedings of the Ocean Drilling Program: Scientific Results* 144, 547–557.
- Reboulet, S., Hoedemaeker, P.J., Aguirre-Urreta, M.B., Alsen, P., Atrops, F., Baraboshkin, E., Company, M., Delanoy, G., Dutour, Y., Klein, J., Latil, J.L., Lukeneder, A., Mitta, V., Mourgues, F.A., Ploch, I., Raisossadat, N., Ropolo, P., Sandoval, J., Tavera, J.M., Vasicek, Z., Vermeulen, J., 2006. Report on the 2nd international meeting of the IUGS lower Cretaceous ammonite working group, the ‘Kilian Group’ (Neuchâtel, Switzerland, 8 September 2005). *Cretaceous Research* 27, 712–715.
- Selby, D., Mutterlose, J., Condon, D.J., 2009. U- Pb and Re-Os geochronology of the Aptian/Albian and Cenomanian/Turonian stage boundaries: Implications for timescale calibration, osmium isotope sea water composition and Re-Os systematics in organic-rich sediments. *Chemical Geology* 265, 394–409.
- Stein, M., Föllmi, K.B., Westermann, S., Godet, A., Adatte, T., Matera, V., Berner, Z., 2011. Progressive palaeoenvironmental change during the late Barremian-early Aptian as prelude to Oceanic Anoxic Event 1a: evidence from the Gorgo a Cerbara section (Umbria-Marche basin, central Italy). *Palaeogeography, Palaeoclimatology, Palaeoecology* 302, 396–406.
- Stoll, H.M., 2016. Aptian mystery solved. *Nature Geoscience* 9, 95–96.
- Sussman, G.J., Wisdom, J., 1992. Chaotic evolution of the Solar System. *Science* 257, 56–62.
- Thomson, D.J., 1982. Spectrum estimation and harmonic-analysis. *Proceedings of the IEEE* 70, 1055–1096.
- Vermeulen, J., 2002. Etude stratigraphique et paléontologique de la famille des Pulchelliidae (ammonoidea, Ammonitina, Endemocerataceae). In: *Laboratoire de Géologie de l'Université I de Grenoble (ed.), Géologie Alpine*. Grenoble, France, p. 333 (2002).
- Westerhold, T., Röhl, U., Frederichs, T., Agnini, C., Raffi, I., Zachos, J.C., Wilkens, R.H., 2017. Astronomical calibration of the Ypresian time scale: Implications for seafloor spreading rates and the chaotic behaviour of the Solar System? *Climate of the Past* 13, 1129–1152.

- Westermann, S., Stein, M., Matera, V., Fiet, N., Fleitmann, D., Adatte, T., Föllmi, K.B., 2013. Rapid changes in the redox conditions of the western Tethys Ocean during the early Aptian oceanic anoxic event. *Geochimica et Cosmochimica Acta* 121, 467–486.
- Westphal, H., 2006. Limestone–marl alternations as environmental archives and the role of early diagenesis: a critical review. *Int. J. Earth Sci. (Geol. Rundsch.)* 95, 947–961.
- Wilpshaar, M., Leereveld, H., Visscher, H., 1997. Early Cretaceous sedimentary and tectonic development of the Dauphinois Basin (SE France). *Cretaceous Research* 18, 457–468.
- Zeebe, R.E., Lourens, L., 2019. Solar system chaos and the Paleocene-Eocene boundary age constrained by geology and astronomy. *Science* 365, 926-929.
- Zeebe, R.E., Lourens, L., 2022. A deep-time dating tool for Paleo-applications utilizing obliquity and precession cycles: The role of dynamical ellipticity and tidal dissipation. *Paleoceanography and Paleoclimatology* 37, e2021PA004349.
- Zhang, Y., Ogg, J.G., Minguetz, D., Hounslow, M.W., Olausson, S., Gradstein, F.M., Esmeray-Senlet, S., 2021. Magnetostratigraphy of U-Pb dated boreholes in Svalbard, Norway, implies that magnetochron M0r (a proposed Barremian-Aptian boundary marker) begins at 121.2±0.4 Ma. *Geology* 49, 733-737.

on the interval between the *Imerites giraudi* Zone (upper Barremian) and the *Deshayesites oglandensis* Zone (lowermost Aptian) (Fig. S2).

1.2. Saut du loup succession

The Saut du loup section is located 18 km to the west of the Angles succession (coordinates: 43°57'38.6"N; 6°20'26.4"E). It consists of rhythmically alternations of marls and mudstones from the *Heinzia sayni* to the *Imerites giraudi* Zones (upper Barremian) (Vermeulen, 2002). This time interval appears more complete than the Angles succession marked by a condensed interval, which permits to build up the continuous succession of the uppermost Barremian (Vermeulen, 1980, 2002; Bodin et al., 2006). Here, we focus on the interval between the *G. sartousiana* and the *M. saranisi* Zone (upper Barremian) (Fig. S2).

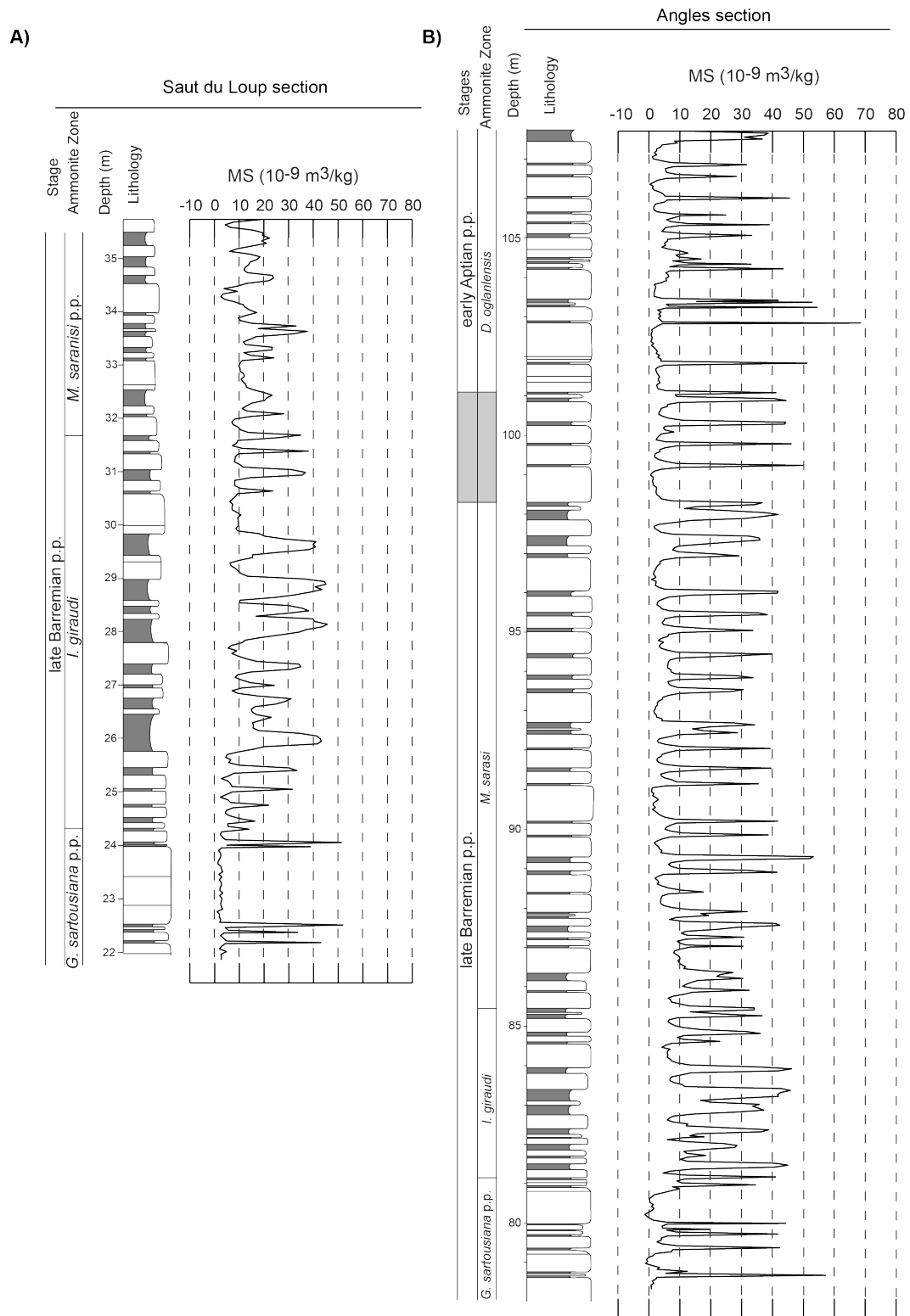


Fig. S2. Biostratigraphy, lithology, and magnetic susceptibility (MS) variations of the late Barremian-early Aptian Saut du Loup and Angles sections. (A) Ammonite zonation, lithology, and MS variations along the Saut du Loup section. (B) Ammonite zonation, lithology, and MS variations along the Angles section.

1.3. Combe Lambert succession

The Combe Lambert succession is located 1 km north of the Angles section (coordinates: 43°56'39.32"N; 6°32'32.97"E). It consists of rhythmical alternations of bioturbated white to grey limestone and grey to dark marls. The top of the section is characterized by the first meters of the blue-grey marl formation. The section is the subject of detailed biostratigraphic investigations based on ammonite biozonation between the *Deshayesites oglanlensis* and the *Deshayesites forbesi* Zones. (Delanoy, 1998; Vermeulen, 2002) (Fig. S3).

1.4. Glaise succession

The Glaise section, close to Veynes (department of "Drôme", coordinates: 44°34'07.09"N; 5°49'00.63"E), is situated in the northeastern part of the basin. It is composed of 33 m thick hemipelagic blue-grey marl succession ("Marne Bleue" Formation), which includes a series of laminated organic-rich layers (Goguel level, 12 m) representing the local expression of the early Aptian Selli oceanic anoxic event (OAE1a). The monotonous marlstone succession is interrupted by centimetric turbiditic layers. The top of the section is marked by two marly limestone beds ("Niveau Blanc"), which represent a basin-wide marker horizon (Bréhéret, 1997). This section is well dated by ammonite covering the *Deshayesites deshayesi*-*Deshayesites furcata* ammonite zones (Bréhéret, 1997) and benefits from high-resolution carbon isotope stratigraphy (Westermann et al., 2013; This study) (Fig. S3).

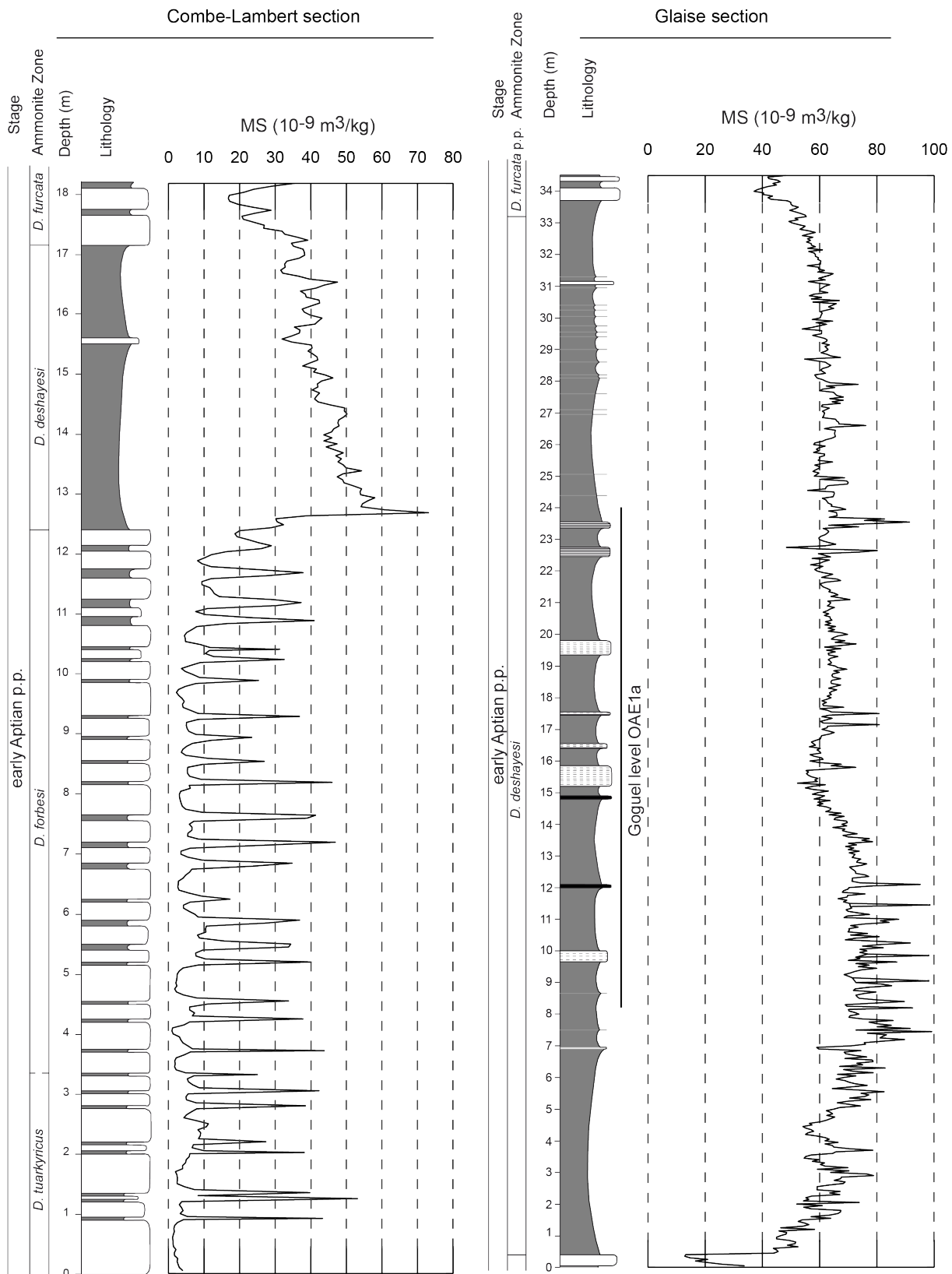


Fig. S3. Biostratigraphy, lithology, and magnetic susceptibility (MS) variations of the Early Aptian Combe-Lambert and Glaise sections. (A) Ammonite zonation, lithology, and MS variations along the Combe-Lambert section. (B) Ammonite zonation, lithology, and MS variations along the Glaise section.

1.5. Serre Chaitieu succession

The section of Serre Chaitieu, close to Lesches en Diois (department of “Drôme”, coordinates: 44°35'13.94"N; 5°31'44.55"E), is located in the northwestern part of the basin. The lithological succession is composed of marlstone, which is briefly interrupted by marly limestone beds (“Niveau Blanc”, “Niveau Calcaire”, and “Niveau noir calcaire”), by pluri-centimetric calciturbidite above the “Niveau Blanc”, and by a weathered volcanic ash layer (“Bentonite Van Gogh”; [Beaudoin et al., 1998](#)). The marlstone interval is punctuated by two organic matter-rich horizons, the “Niveau Noir” and “Niveau Fallot”. The temporal framework is well defined by ammonite, planktonic foraminifera, and nannofossils biostratigraphy ([Bréhéret, 1997](#); [Dauphin, 2002](#); [Herrle and Mutterlose, 2003](#); [Herrle et al., 2004](#); [Dutour, 2005](#)). Here, we focus on the interval between the “Niveau Blanc” and the “Niveau Fallot”, which encompasses the *Deshayesites furcate*-*Epicheloniceras martini* Zones (Fig. S4).

1.6. Beaudinard succession

The Beaudinard section, close to Reynier (coordinates: 44°18'26.27"N; 6°08'02.38"E), is situated in the central part of the basin. The outcrop is composed of 230 m thick of blue-grey marl of the “Marne bleue” formation, which includes the “Niveau Fallot”, a centimetric turbiditic layer, and a weathered volcanic ash layer (“Matisse” bentonite; [Beaudoin et al., 1998](#)). The top of the section is characterized by bioturbated limestones alternating with marls: the “Faisceau Nolan” and “Faisceau Fromaget”. It is well dated by ammonoids, planktonic foraminifera, and calcareous nannofossils ([Bréhéret, 1997](#); [Herrle et al., 2003](#); [Dutour, 2005](#)) (Fig. S4).

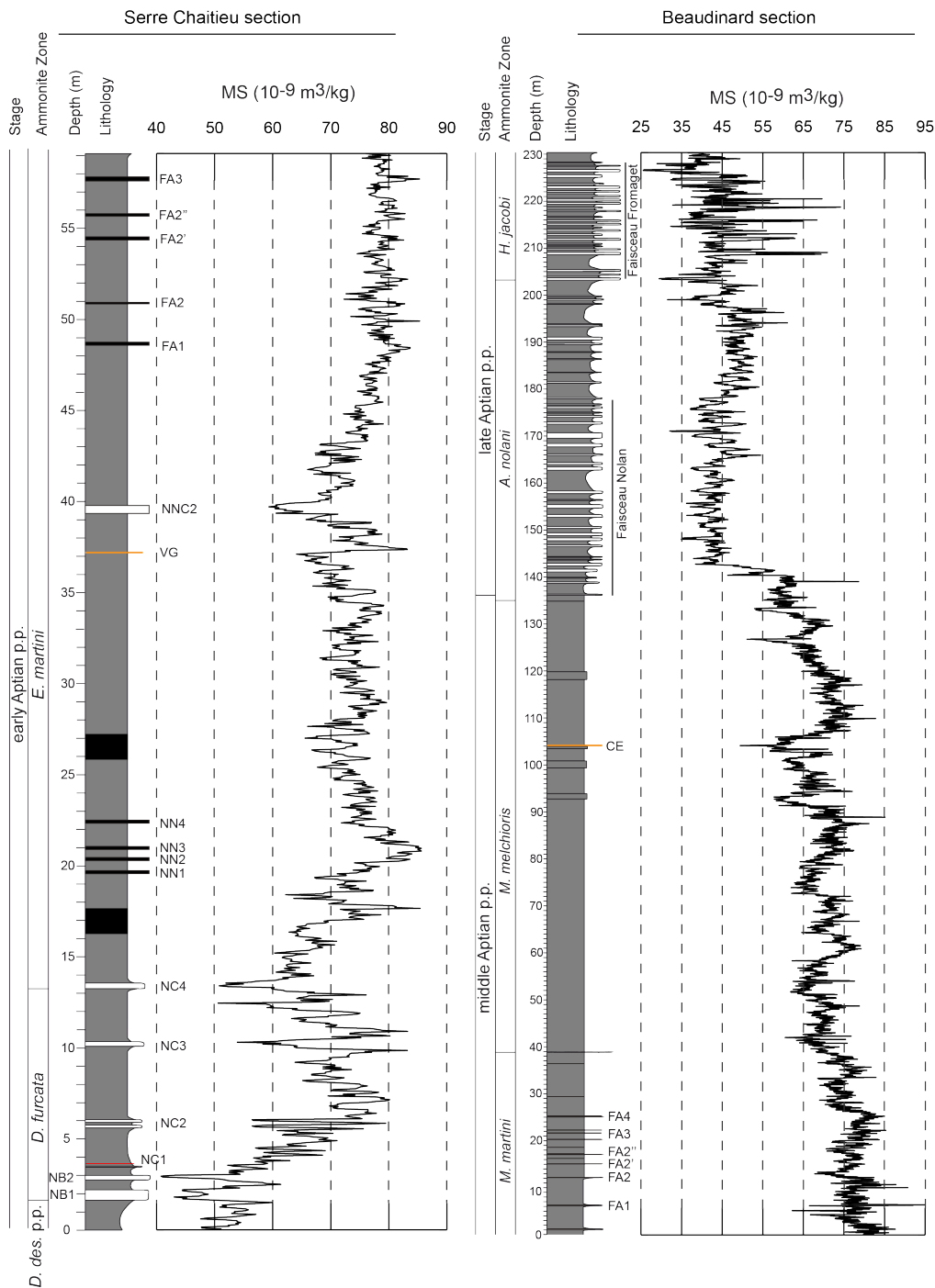


Fig. S4. Biostratigraphy, lithology, and magnetic susceptibility (MS) variations of the Early Aptian-Late Aptian Serre Chaitieu and Beaudinard sections. (A) Ammonite zonation, lithology, and MS variations along the Serre Chaitieu section. (B) Ammonite zonation, lithology, and MS variations along the Beaudinard section.

1.7. Col de Pré-Guittard succession

The Col de Pré-Guittard section, close to Arnanon (department of “La Drôme”, coordinates: 44°30'29.43"N; 5°17'50.83"E), is located in the northwestern part of the Vocontian Basin (Fig. 1). This site represents the Global Stratotype Section and Point (GSSP) for the base of the Albian (Kennedy et al., 2017), spanning the uppermost Aptian to the lowermost Albian interval. The lithological succession is composed of marlstone, which is interrupted by rhythmic marl-limestone

alternation at the base (“Faisceau Fromaget”), and by marly limestone beds (“Délit Calcaire”). This interval includes two organic-rich horizons: the Niveau Jacob and Kilian, which represent the sedimentary expression of the oceanic anoxic event 1b. The temporal framework is well defined by ammonite, planktonic foraminifera, and nannofossils biostratigraphy ([Bréhéret, 1997](#); [Herrle and Mutterlose, 2003](#); [Herrle et al., 2003](#); [Kennedy et al., 2000, 2017](#)) (Fig. S5).

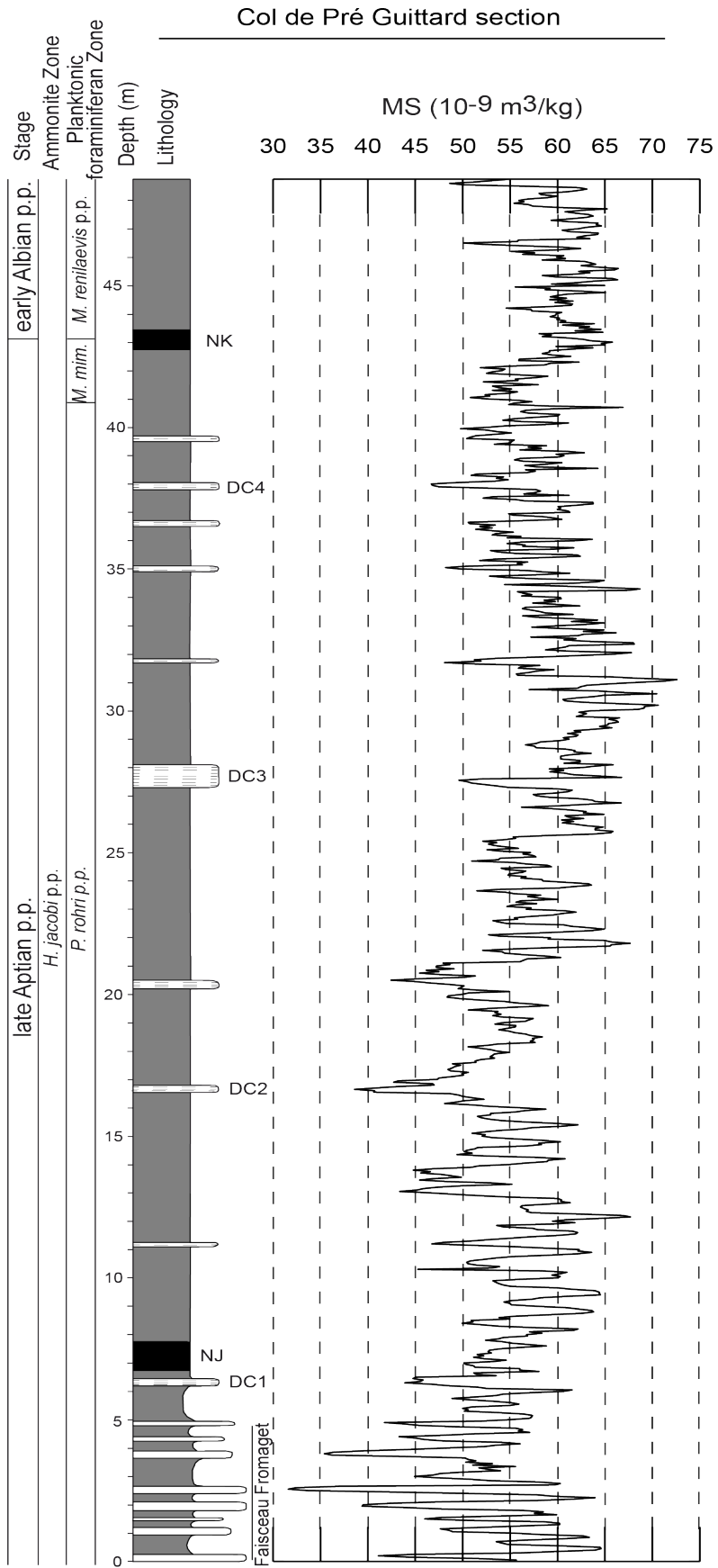


Fig. S5. Biostratigraphy, lithology, and magnetic susceptibility (MS) variations of the Late Aptian-Early Albian Col de Pré-Guittard section.

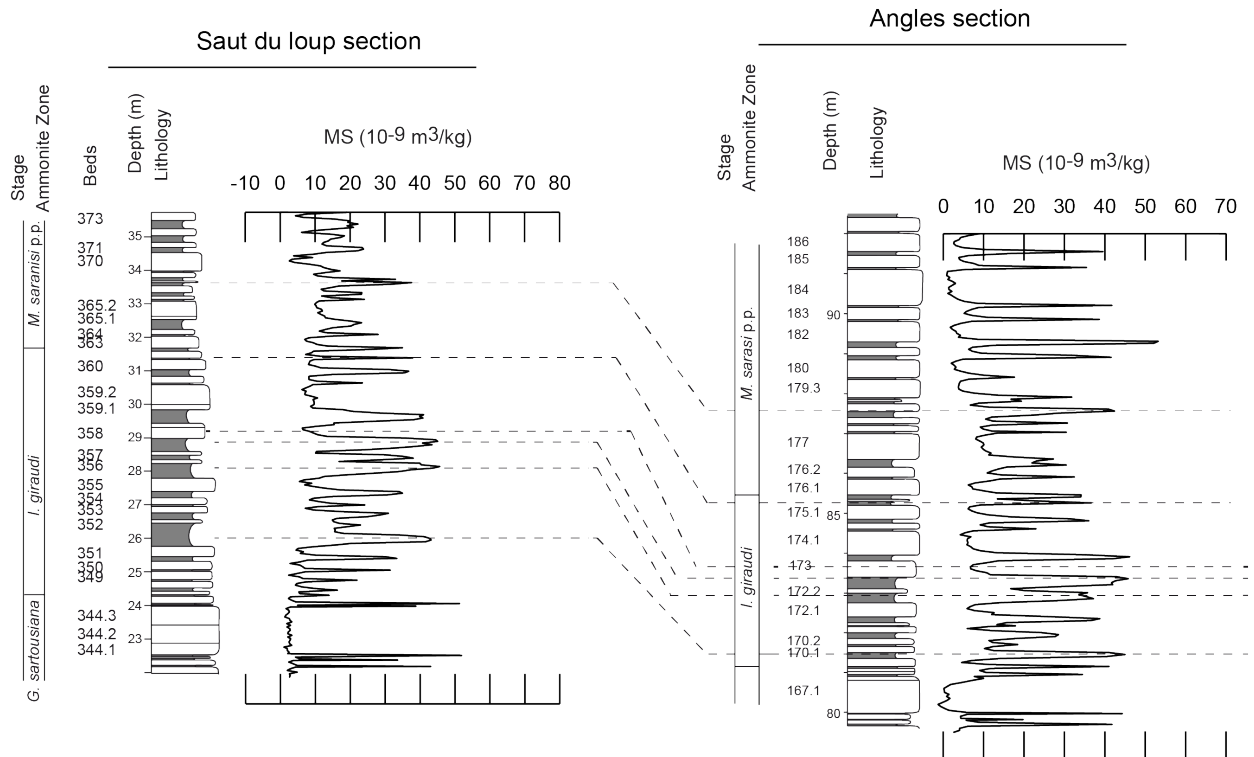


Fig. S6. Lithostratigraphic, biostratigraphic, and magnetic susceptibility correlations between the sections of Angles and Saut du Loup.

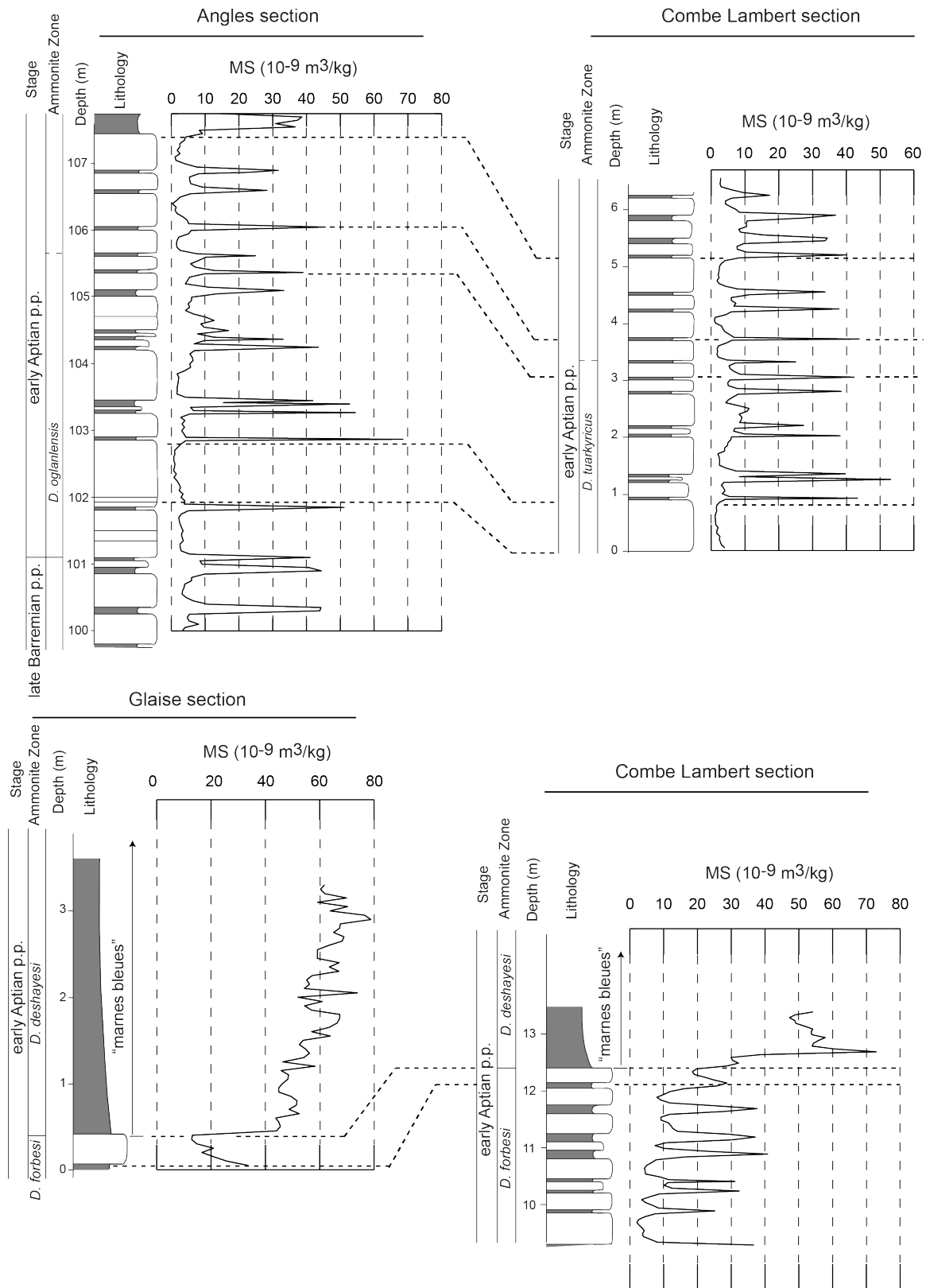


Fig. S7. Lithostratigraphic, biostratigraphic, and magnetic susceptibility correlations between the sections of Angles and Combe-Lambert, and between the sections of Combe-Lambert and Glaise.

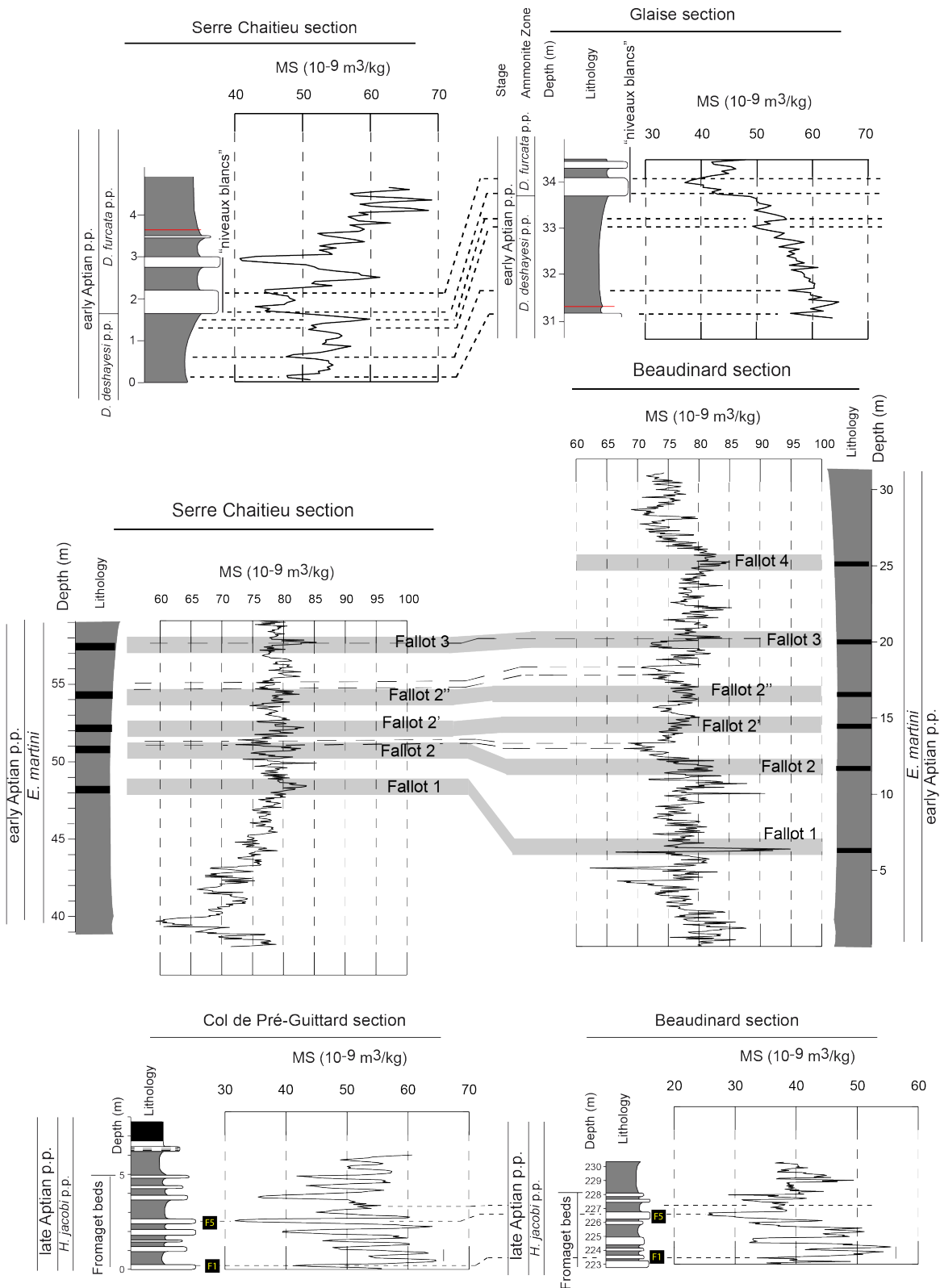


Fig. S8. Lithostratigraphic, biostratigraphic, and magnetic susceptibility correlations between the sections of Glaise and Serre Chaitieu, between the sections of Serre Chaitieu and Beaudinard, and between the sections of Beaudinard and Col de Pré-Guittard.

Vocontian Basin

Composite section

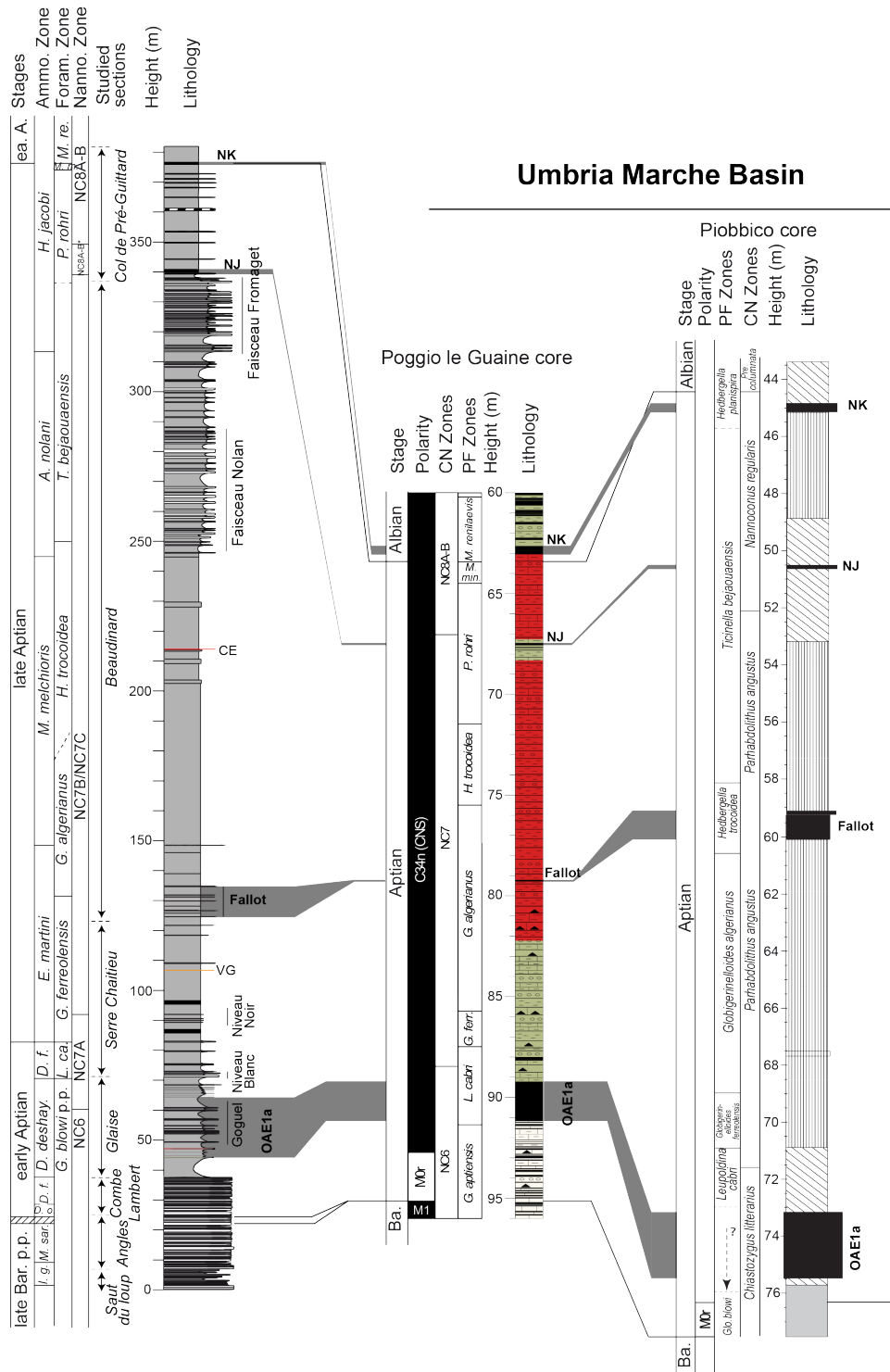
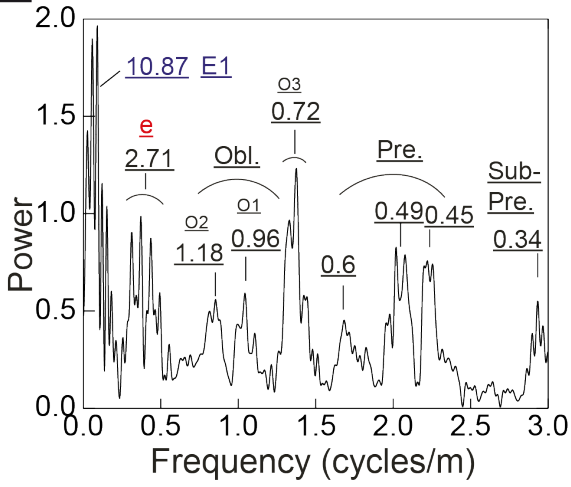


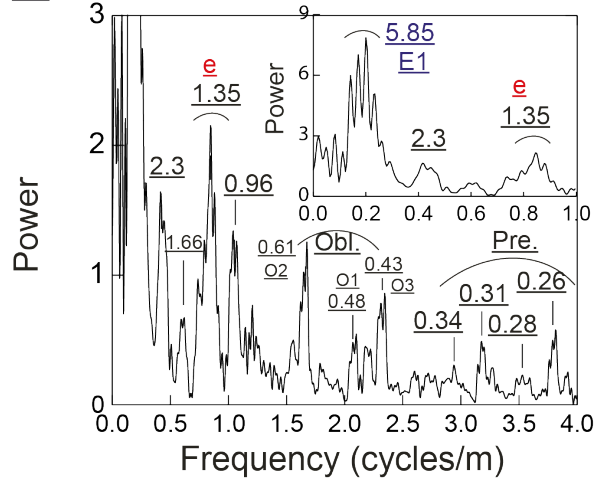
Fig. S9. Biostratigraphy, magnetostratigraphy, lithology records of the sections and cores from the composite section in the Vocontian Basin (This study), the Poggio le Guaine core in the Umbria Marche Basin (Leandro et al., 2022), and the Piobbico core in the Umbria Marche Basin (Huang et al., 2010).

2. Spectral analysis and orbital tuning

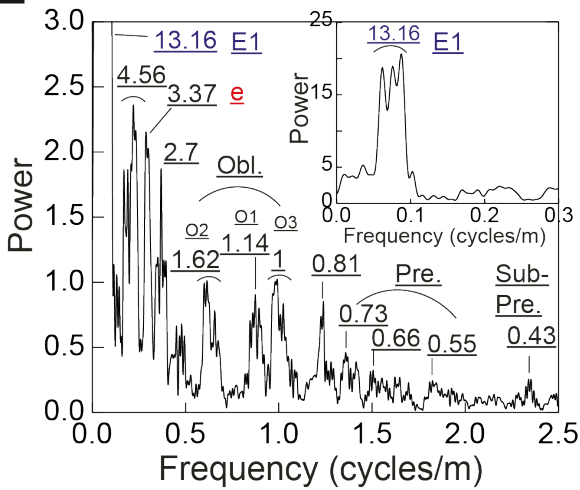
11



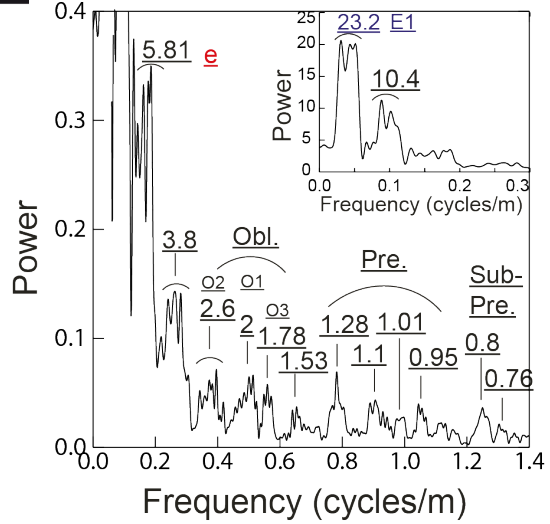
12



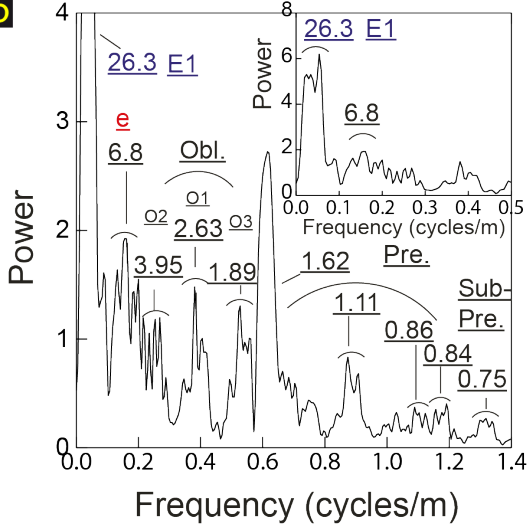
13



14



15



16

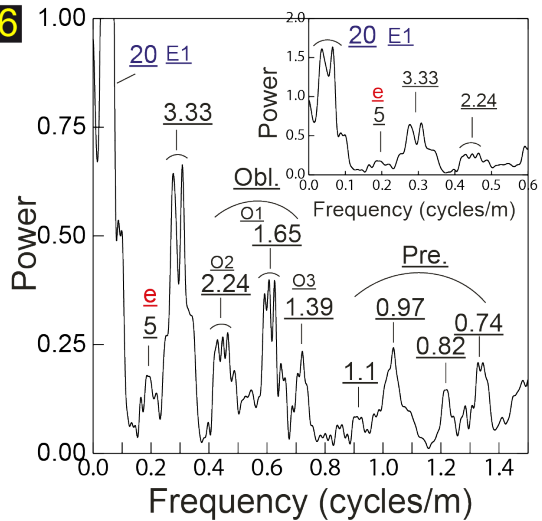


Fig. S10. 2π -MTM power spectra of magnetic susceptibility data of the composite succession, SE France. **A)** Raw MS data of the interval 0 to 39 m, with the high-power peaks in the low frequencies truncated to emphasize the high-frequency portion of the spectrum. *Inset:* spectrum over [0, 0.4 cycles/m]. **B)** Raw MS data of the interval 34 to 75 m, with the high-power peaks in the low frequencies (17.86- and 5.85-m wavelengths) truncated to emphasize the high-frequency portion of the spectrum. *Inset:* spectrum over [0, 0.7 cycles/m]. **C)** Raw MS data of the interval 69.4 to 163 m, with the high-power peak in the low frequencies (13.16-m wavelengths) truncated to emphasize the high-frequency portion of the spectrum. *Inset:* spectrum over [0, 0.3 cycles/m]. **D)** Raw MS data of the interval 155 to 260 m, with the high-power peaks in the low frequencies (22.7-, and 10.4-m wavelengths) truncated to emphasize the high-frequency portion of the spectrum. *Inset:* spectrum over [0, 0.3 cycles/m]. **E)** Raw MS data of the interval 250 to 315 m, with the high-power peaks in the low frequencies (29.4-, and 6.8-m wavelengths) truncated to emphasize the high frequency portion of the spectrum. *Inset:* spectrum over [0, 0.5 cycles/m], and **F)** Raw MS data of the interval 310 to 382 m, with the high-power peaks in the low frequencies (20-, 5-, and 3.33-m wavelengths) truncated to emphasize the high-frequency portion of the spectrum. *Inset:* spectrum over [0, 0.3 cycles/m]. Abbreviations: “Sub-Pre.” for sub-precession, “Pre.” for precession, “Obl.” for obliquity, “e” for short eccentricity, and “E1” for g2-g5 (405-kyr) eccentricity term.

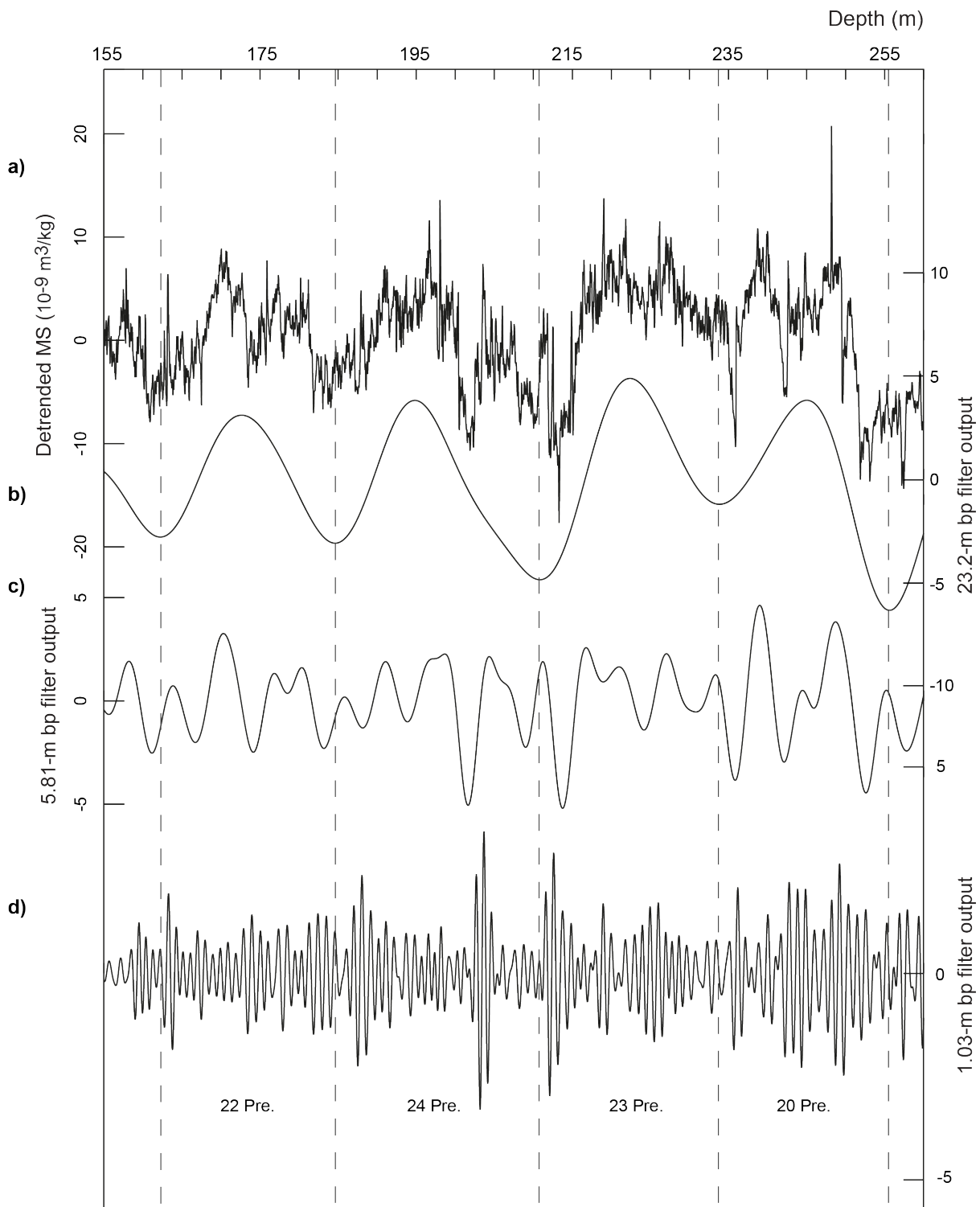


Fig. S11. Detail of the Early Aptian interval showing the cyclic variations of MS values from 250 to 315 m (interval I5). **a)** Detrended MS variations with a 30% weighted average smoothing. **b)** Gaussian bandpass filter output to isolate 23.2 cycles-m (0.043 ± 0.03 cycles-m). **c)** Gaussian bandpass filter output to isolate 5.81-m (0.172 ± 0.1 cycles-m). **d)** Gaussian bandpass filter output to isolate 1.03-m (0.97 ± 0.3 cycles-m). The gaussian bandpass filter are interpreted as reflecting the 405-kyr eccentricity, the short eccentricity cycles, and the precession cycles respectively. Abbreviations: “Pre.” for the precession cycles.

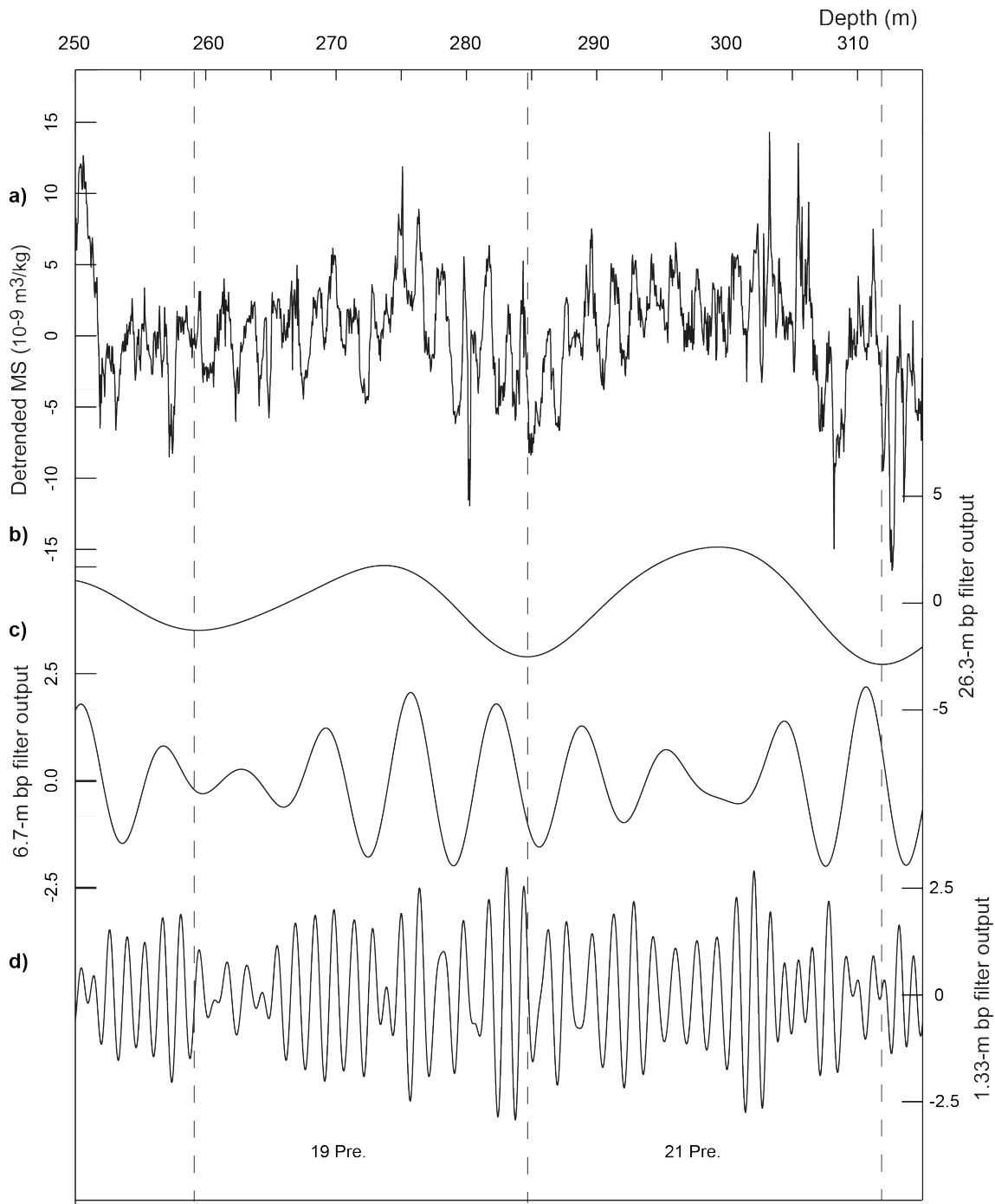


Fig. S12. Detail of the Early Aptian interval showing the cyclic variations of MS values from 155 to 260 m. **a)** Detrended MS variations with a 30% weighted average smoothing. **b)** Gaussian bandpass filter output to isolate 26.3 cycles-m (0.038 ± 0.03 cycles-m). **c)** Gaussian bandpass filter output to isolate 6.7-m (0.15 ± 0.04 cycles-m). **d)** Gaussian bandpass filter output to isolate 1.3-m (0.75 ± 0.2 cycles-m). The gaussian bandpass filter are interpreted as reflecting the 405-kyr eccentricity, the short eccentricity cycles, and the precession cycles respectively. Abbreviations: “Pre.” for the precession cycles.

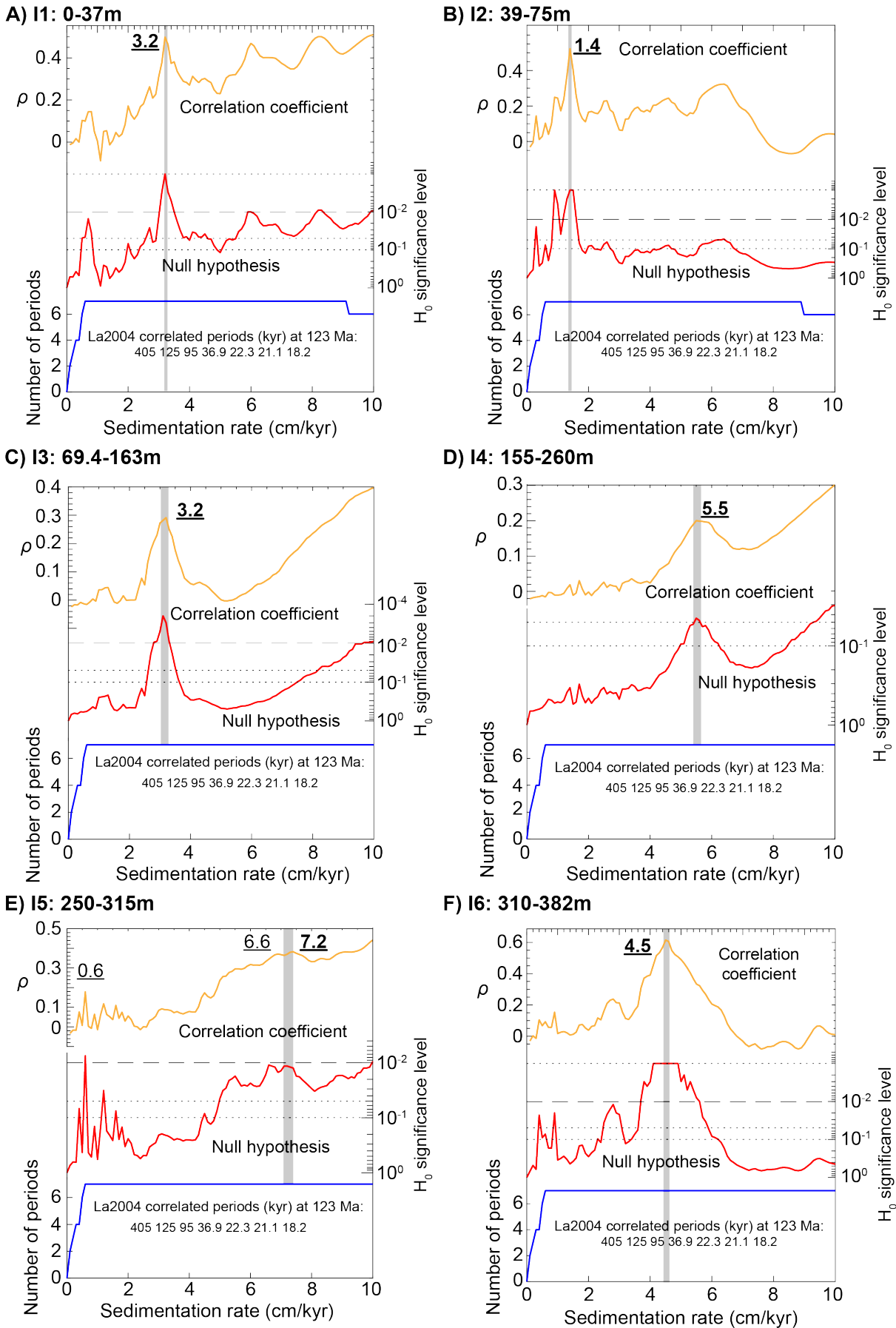


Fig. S13. The correlation coefficient results (COCO technique, Li et al., 2018; see Methods) per intervals, used to test the optimal sedimentation rates of orbitally forced MS variations. (A) Interval I1:

Raw 0-37 m. (B) Interval I2: 25% weighted average detrended 39-75 m. (C) Interval I3: Raw 70-163 m. (D) Interval I4: Raw 155-260 m. (E) Interval I5: Raw 250-315 m. (F) Interval I6: 45% weighted average detrended 310-382.05 m. COCO outputs, the Pearson correlation coefficient (orange line), the null hypothesis results (red line, Null hypothesis of no astronomical forcing, H_0), and the number of contributing astronomical parameters in the target series used to test sedimentation rates (blue curve). Null hypothesis H_0 is estimated via Monte Carlo simulation with 1000 iterations. The astronomical target series is from La2004 astronomical solution (Laskar et al., 2004) with data centred on the Aptian-Albian boundary at nearly 113.2 Ma (Gradstein et al., 2020). The tested COCO sedimentation rates are 0–10 cm/kyr with an increment of 0.1 cm/kyr.

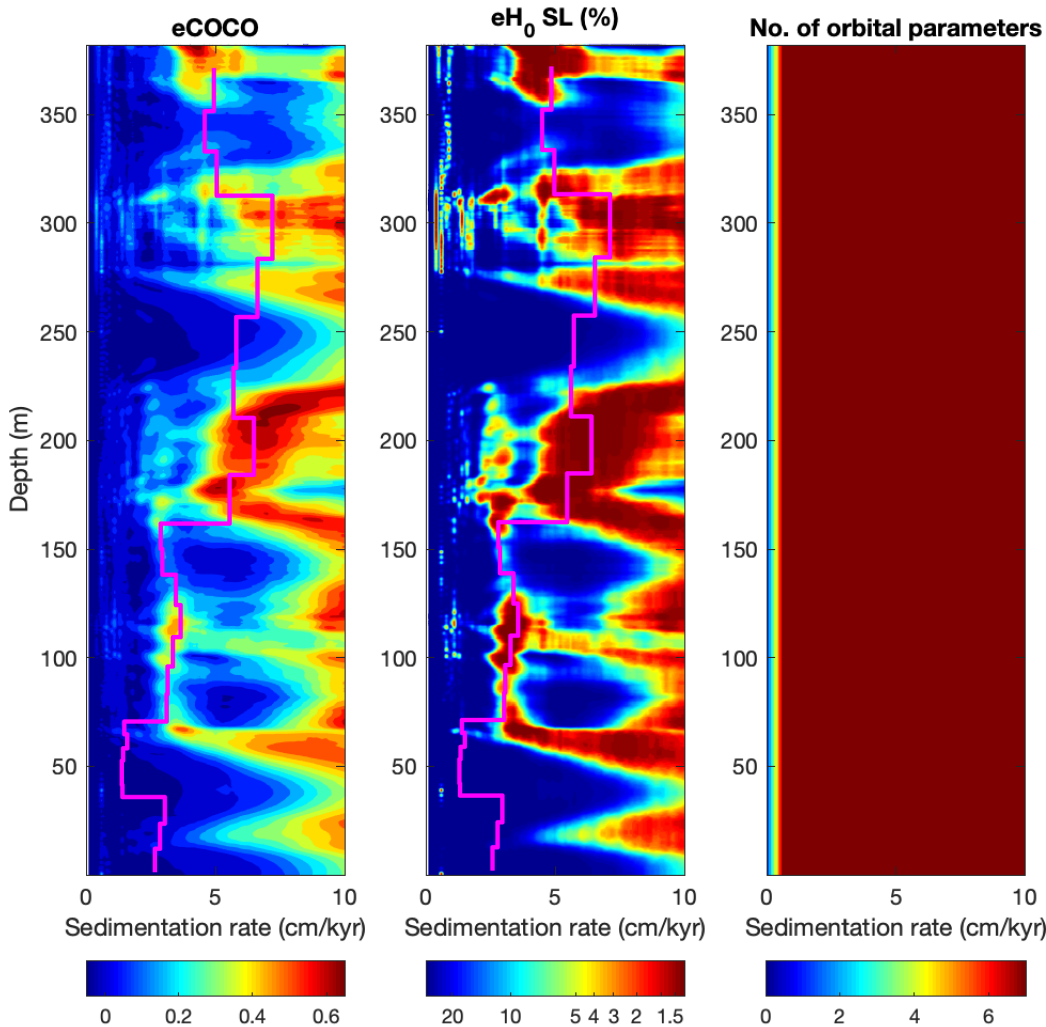


Fig. S14. Statistical evulsive COCO outputs (see Methods) applied to the whole, raw MS data. Left panel: Pearson correlation coefficient, middle panel: null hypothesis H_0 . Stair-like curve in pink is the sedimentation rate inferred from the 405 kyr tuning of visually inspected sediment wavelengths related to the 405 kyr eccentricity term. The eCOCO parameters are 0–10 cm/kyr with an increment of 0.1 cm/kyr for testing sedimentation rates, window = 60 m, step = 0.1 m, 1000 Monte Carlo simulations, La2004 astronomical parameters at 113.2 Ma. Note that the manual sedimentation rate tracks the statistically inferred eCOCO sedimentation rate, except for the basal interval (where the significance is very low), at the transition from the marl-limestone alternations and the marly succession of the “Marnes Bleues” Formation of the lowermost Aptian, encoded by a strong shift in the MS signal (see

main Fig. 3). However, single COCO outputs below and above the MS shift provide highly significant optimal sedimentation rates, again supported by our visual interpretation.

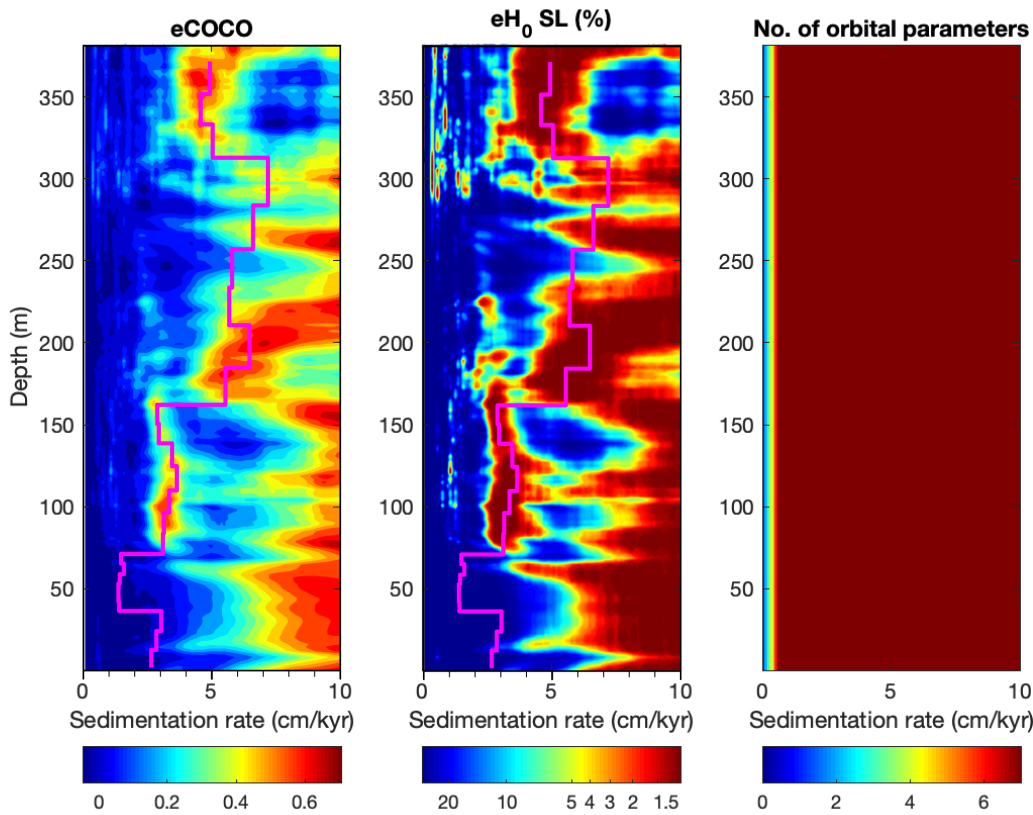


Fig. S15. The same caption as in Supplementary Fig. S14 with the evolutive COCO applied to 15% weighted average LOWESS (see Methods).

3. Durations of the Aptian stage and ammonite zones

Ammonite Zones	This study	Ghirardi et al., 2014	GTS2020
<i>I. giraudi</i>	0.257 Myr		0.46 Myr
<i>M. sarasini</i>	0.462-0.560 Myr		0.4 Myr
<i>D. oglanlensis</i>	0.134-0.231 Myr		0.5 Myr
<i>D. forbesi</i>	0.327 Myr		0.68 Myr
<i>D. deshayesi</i>	2.308 Myr		0.86 Myr
<i>D. furcata</i>	0.427 Myr	0.42 Myr	0.35 Myr
<i>E. martini</i>	1.970 Myr	1.52 Myr	1.23 Myr
<i>M. melchioris</i>	1.885 Myr		0.79 Myr
<i>A. nolani</i>	1.029 Myr		2.37 Myr
Aptian stage	9.4-9.5 Myr		8.2 Myr

Table S1. Comparison of ammonite biozone durations estimate from the astronomical calibration of the composite succession in the Vocontian Basin (This study), from the orbital calibration of the Serre Chaitieu succession (Ghirardi et al., 2014), and GTS2020 (Gradstein et al., 2020).

4. Supplementary results for astronomical model

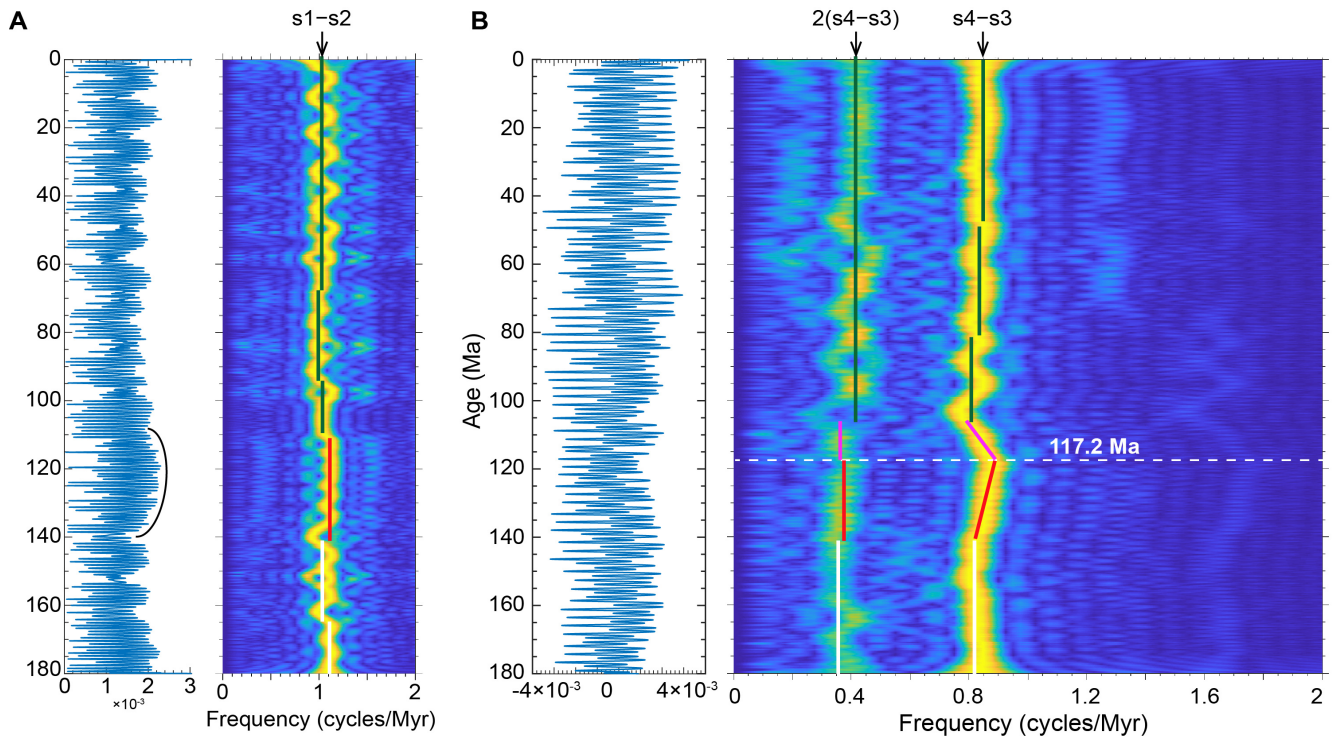


Fig. S16. Testing the mid-Aptian secular resonance in the La2004 inclinations, which occurred at the coupled resonant terms θ , σ (Laskar, 1990, 1992; Sussman and Wisdom, 1992) and σ' (Lithwick and Wu, 2011), see also Mogavero and Laskar (2022) for an update. (A) $s_{\text{Mercury}} - s_{\text{Venus}}$ variation along with its spectrogram. (B) $s_{\text{Mars}} - s_{\text{Earth}}$ variation along with its spectrogram.

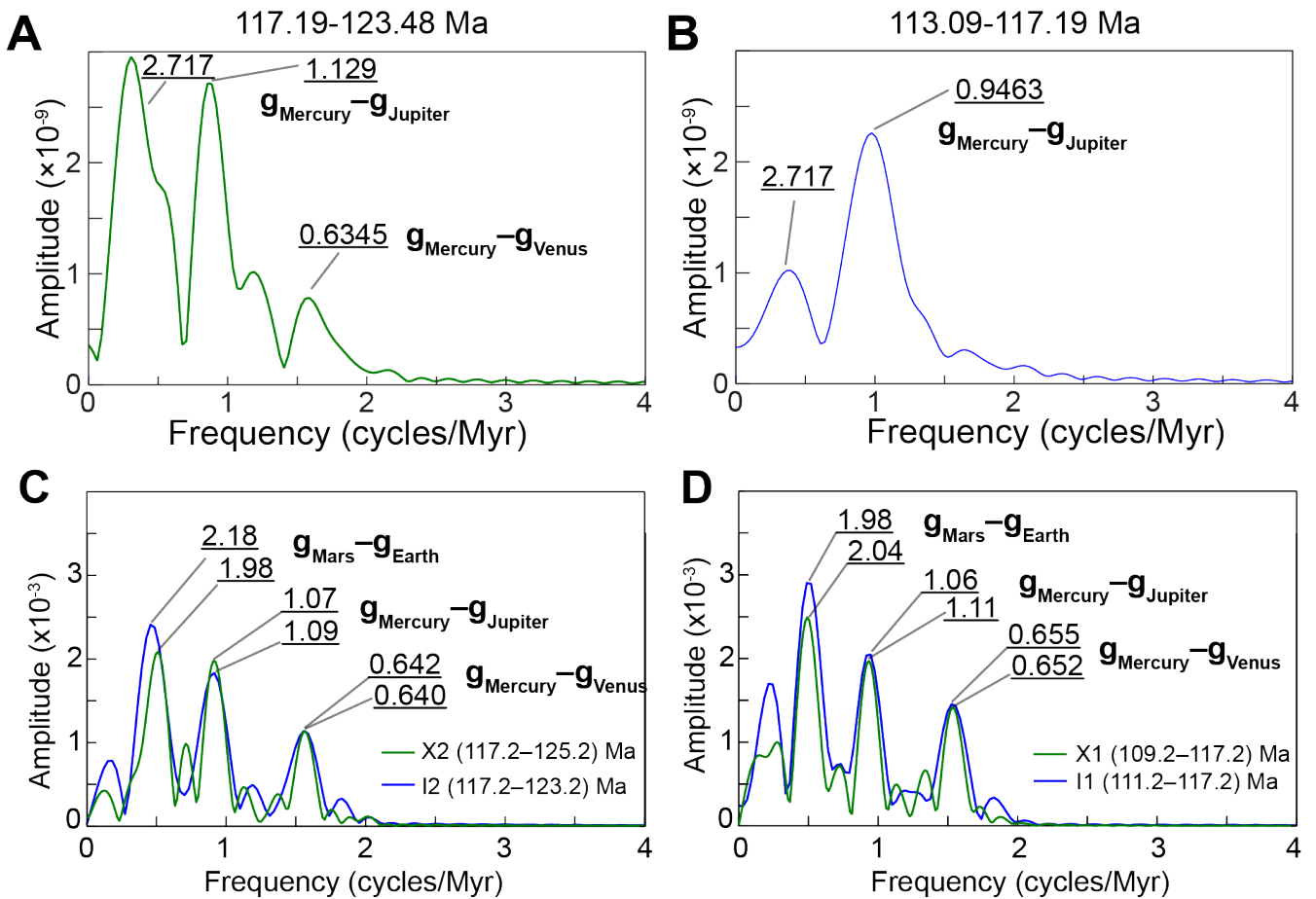


Fig. S17. Time-series analysis of low-frequency variations in Earth's orbital eccentricity of the MS data from the Vocontian Basin (SE France) and the La2004 astronomical model (Laskar et al., 2004). (A) Power spectra of the tuned MS data from 117.19 to 123.48 Ma. (B) Power spectra of the tuned MS data from 113.09 to 117.19 Ma. (C) Power spectra of the La2004 astronomical model from 117.2 to 125.2 Ma and from 117.2 to 123.2 Ma. (D) Power spectra of the La2004 astronomical model from 109.2 to 117.2 Ma and from 111.2 to 117.2 Ma.

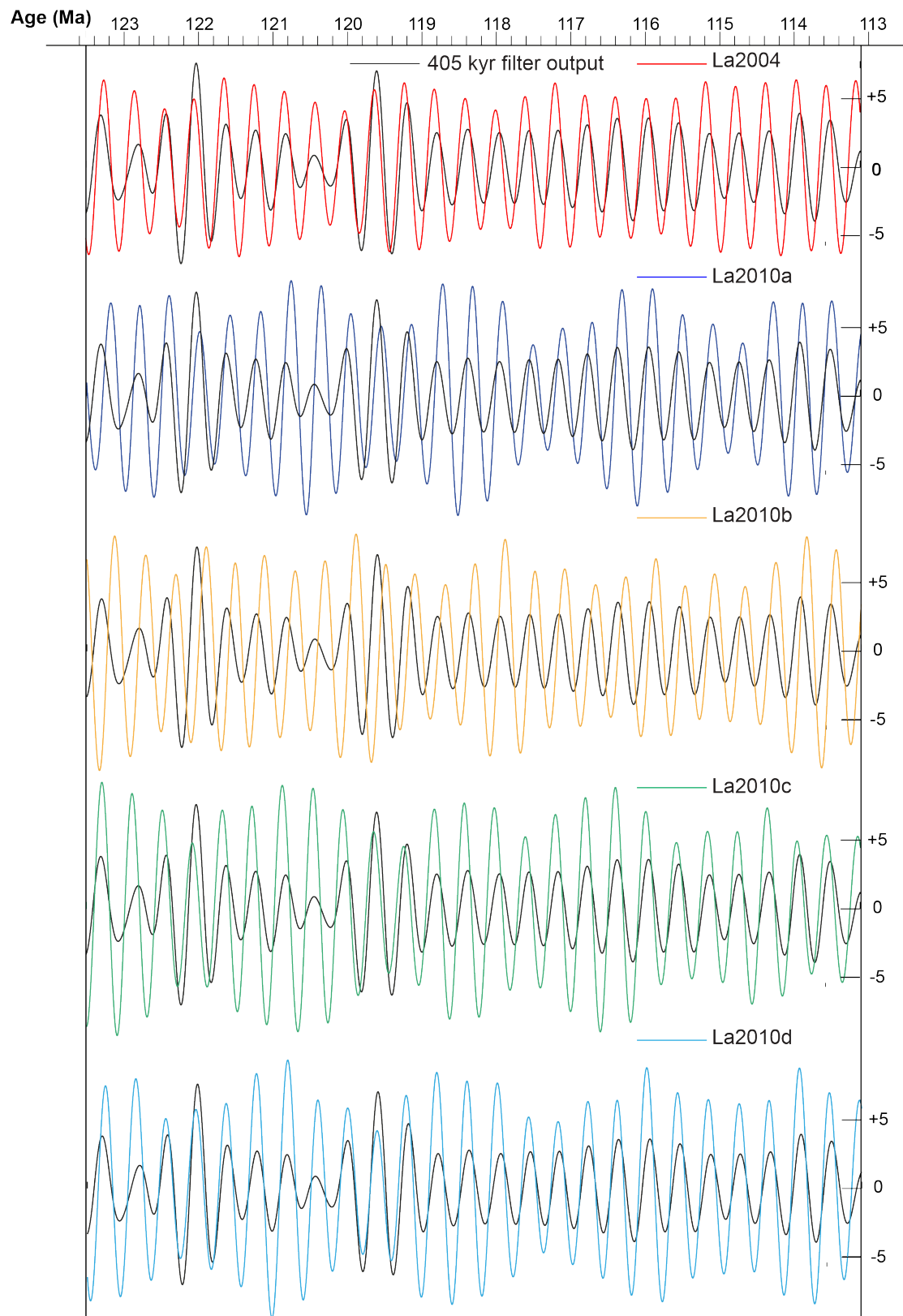


Fig. S18. The g2–g5 (405-kyr) band power extracted from the Vocontian Basin (MS data) (0.0247 ± 0.001 cycles-kyr), and the different bands power extracted from the astronomical solutions (La2004, La2010a, La2010b, La2010c, and La2010d) (0.0247 ± 0.001 cycles-kyr).

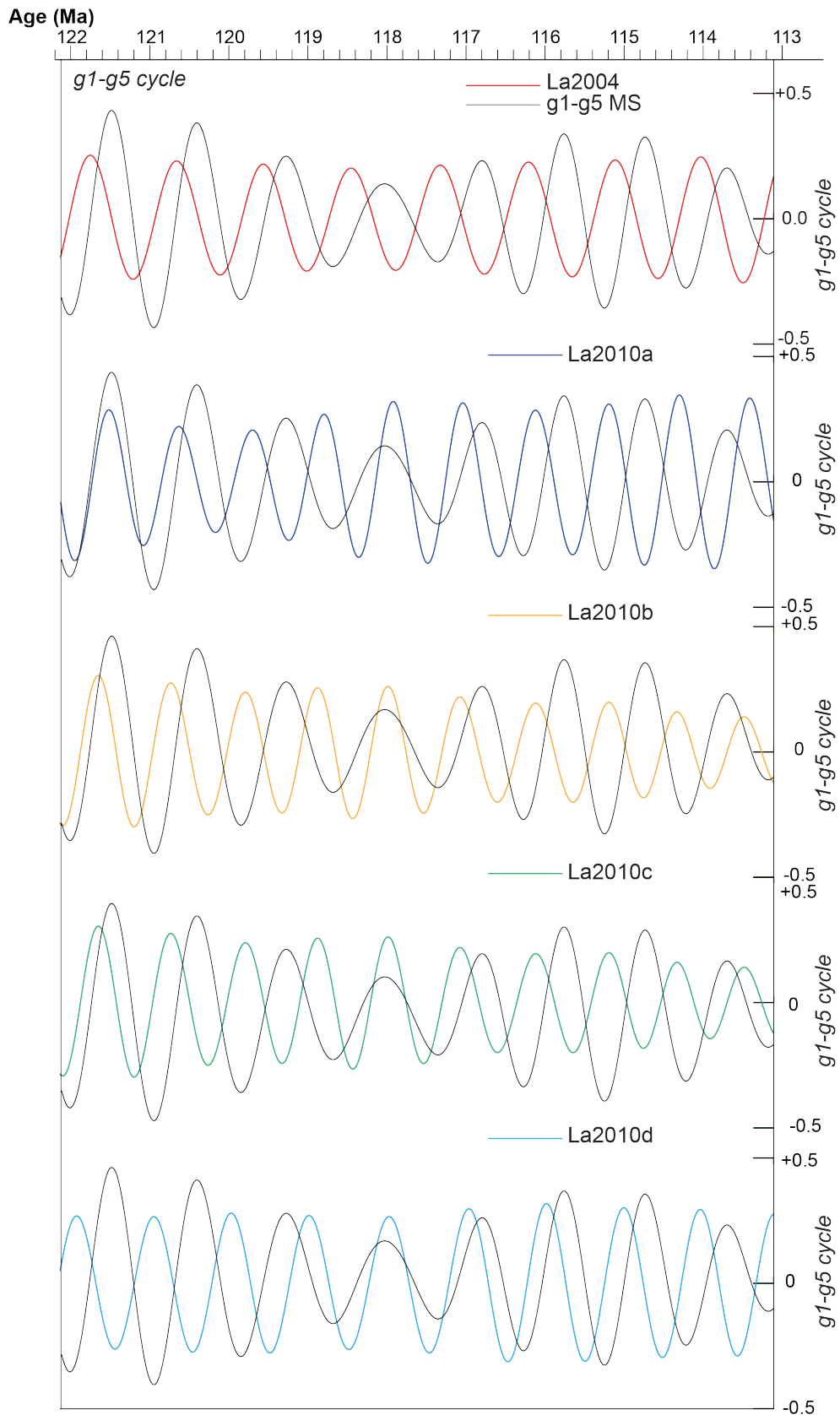


Fig. S19. The $g1-g5$ band power extracted from the Vocontian Basin (MS data) (0.0092 ± 0.002 cycles-kyr), and the different bands power extracted from the astronomical solutions (La2004, La2010a, La2010b, La2010c, and La2010d) (0.0092 ± 0.002 cycles-kyr).

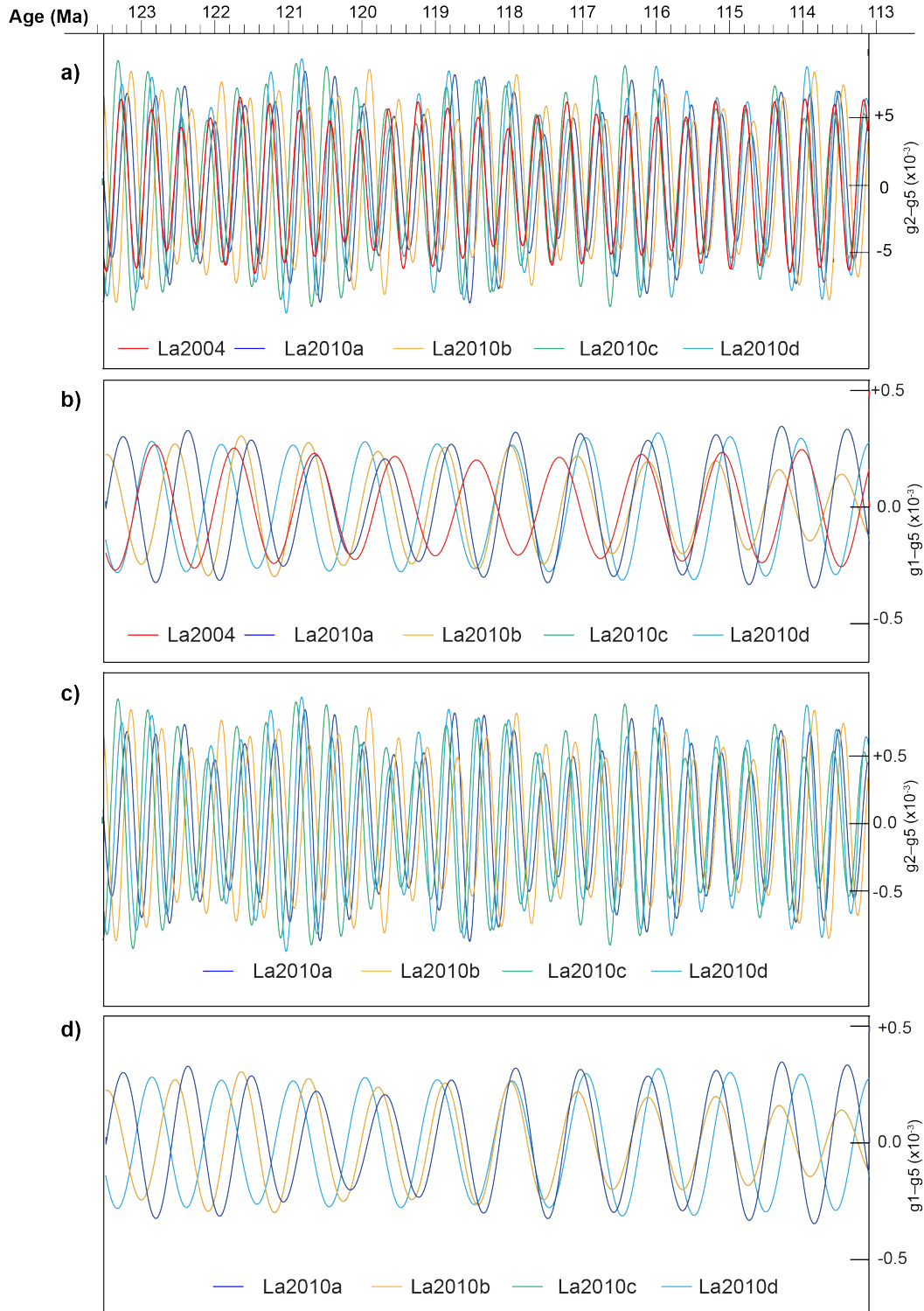


Fig. S20. Long eccentricity (g1–g5 and g2–g5 cycles) band power of orbital solutions. **a)** The g2–g5 (405-kyr) band power extracted from the La2004, La2010a, La2010b, La2010c, and La2010d solutions (0.0247 ± 0.001 cycles-kyr). **b)** The g1–g5 band power extracted from the La2004, La2010a, La2010b, La2010c, and La2010d solutions (0.0092 ± 0.002 cycles-kyr). **c)** The g2–g5 (405-kyr) band power extracted from the La2010a, La2010b, La2010c, and La2010d solutions (0.0247 ± 0.001 cycles-kyr). **d)** The g1–g5 band power extracted from the La2010a, La2010b, La2010c, and La2010d solutions (0.0092 ± 0.002 cycles-kyr).

SI References

- Beaudoin, B., Agassant, J., André, M., Atrops, F., Bahamian, O., Bulot, L., Delattre, M., Dauphin, L., Eckert, S., Friès, G., Guyard, F., Jacquemin, O., Lalande, M., Marcombes, D., Mazingue, V., Parize, O., Pasquier, C., Pinault, M., Reboulet, S., Rosenzweig, F., Rouger, G., Sandamiani, A., Spindler, P., Szymkowski, B., Veret, G., 1998. Les bentonites du Crétacé inférieur du SE de la France. In: Bassin crétacés de France et d'Europe occidentale, Réunion spécialisée de la Société Géologique de France, 6–7 Novembre 1998, Paris, abstract, 8–9.
- Bodin, S., Godet, A., Föllmi, K.B., Vermeulen, J., Arnaud, H., Strasser, A., Fiet, N., Adatte, T., 2006. The late Hauterivian Faraoni oceanic anoxic event in the western Tethys: Evidence from phosphorus burial rate. *Palaeogeography, Palaeoclimatology, Palaeoecology* **235**, 245–264.
- Bréhéret, J.G., 1997. L'Aptien et l'Albien de la Fosse vocontienne (des bordures au bassin). Evolution de la sédimentation et enseignements sur les événements anoxiques. *Société Géologique du Nord*, Mémoire **25**, 164 pp.
- Dauphin, L., 2002. Litho-, bio- et chronostratigraphie comparées dans le Bassin Vocontien, à l'Aptien. Unpublished PhD Thesis, Université des Sciences et Techniques - Lille I, 515 pp.
- Delanoy, G., 1997. Biostratigraphie haute résolution du Barrémien supérieur du sud-est de la France. *Comptes Rendus de l'Académie des Sciences-Série IIA-Earth and Planetary Science* **325**, 689–694.
- Delanoy, G., 1998. Biostratigraphie des faunes d'ammonites à la limite Barrémien–Aptien dans la région d'Angles–Barrême–Castellane. Etude particulière de la famille des Heteroceratina Spath, 1922 (Ancyloceratina, Ammonoidea). *Annales du Muséum d'Histoire Naturelle de Nice* **tomé XII**, 1–270.
- Dutour, Y., 2005. Biostratigraphie, évolution et renouvellements des ammonites de l'Aptien supérieur (Gargasien) du bassin vocontien (Sud-Est de la France). Thèse de Doctorat. Université Claude Bernard - Lyon I pp 201.
- Ghirardi, J., Deconinck, J.F., Pellenard, P., Martinez, M., Bruneau, L., Amiotte-Suchet, P., Pucéat, E., 2014. Multi-proxy orbital chronology in the aftermath of the Aptian Oceanic Anoxic Event 1a: Palaeoceanographic implications (Serre Chaitieu section, Vocontian Basin, SE France). *Newsletters on Stratigraphy* **47**, 247–262.
- Godet, A., Bodin, S., Föllmi, K.B., Vermeulen, J., Gardin, S., Fiet, N., Adatte, T., Berner, Z., Stüben, D., Van de Schootbrugge, B., 2006. Evolution of the marine stable carbon- isotope record during the early Cretaceous: a focus on the late Hauterivian and Barremian in the Tethyan realm. *Earth Planet. Sci. Lett.* **242**, 254–271.
- Gradstein, F.M., Ogg, J.G., Schmitz, M.D., Ogg, G.M., 2020. The Geologic Time Scale 2020, 2 volumes, 1390 pp. doi.org/10.1016/C2020-1-02369-3.
- Herrle, J.O., 2003. Reconstructing nutricline dynamics of Mid-Cretaceous oceans: Evidence from calcareous nannofossils from the Niveau Paquier black shale (SE France). *Marine Micropaleontology* **47**, 307–321.
- Herrle, J.O., Mutterlose, J., 2003. Calcareous nannofossils from the Aptian–early Albian of SE France: paleoecological and biostratigraphic implications. *Cretaceous Research* **24**, 1–22.
- Herrle, J.O., Pross, J., Friedrich, O., Köbller, P., Hemleben, C., 2003. Forcing mechanisms for mid-Cretaceous black shale formation: evidence from the Upper Aptian and Lower Albian of the Vocontian Basin (SE France). *Palaeogeography, Palaeoclimatology, Palaeoecology* **190**, 399–426.
- Herrle, J.O., Köbller, P., Friedrich, O., Erlenkeuser, H., Hemleben, C., 2004. High-resolution carbon isotope records of the Aptian to Lower Albian from SE France and the Mazagan Plateau (DSDP Site 545): a stratigraphic tool for paleoceanographic and paleobiologic reconstruction. *Earth and*

Planetary Science Letters **218**, 149–161.

- Huang, C., Hinnov, L., Fischer, A.G., Grippo, A., Herbert, T., 2010. Astronomical tuning of the Aptian stage from Italian reference sections. *Geology* **38**, 899–902.
- Kennedy, J.W., Gale, A.S., Bown, P.R., Caron, M., Davey, R.J., Gröcke, D., Wray, D.S., 2000. Integrated stratigraphy across the Aptian-Albian boundary in the Marnes Bleues at the Col de Pré-Guittard, Arnayon (Drôme), and at Tartonne (Alpes de Haute Provence), France: A candidate Global-Boundary-Stratotype Section and Boundary Point for the base of the Albian stage. *Cretaceous Research* **21**, 591–720.
- Kennedy, J.W., Gale, A.S., Huber, B.T., Petrizzo, M.R., Bown, P., Jenkyns, H.C., 2017. The global boundary stratotype section and point (GSSP) for the base of the Albian stage, of the Cretaceous, the Col de Pré-Guittard section, Arnayon, Drôme, France. *Episodes* **40**, 177–188.
- Laskar, J., 1990. The chaotic motion of the Solar System: a numerical estimate of the size of the chaotic zones. *Icarus* **88**, 266–291.
- Laskar, J., 1992. La stabilité du Système Solaire, in Chaos et Déterminisme, A. Dahan et al., eds., Seuil, Paris.
- Laskar, J., Robutel, P., Joutel, F., Gastineau, M., Correia, A.C.M., Levrard, B., 2004. A long-term numerical solution for the insolation quantities of the Earth. *Astronomy & Astrophysics* **428**, 261–285.
- Leandro, C.G., Savian, J.F., Kochhann, M.V.L., Franco, D.R., Coccioni, R., Frontalini, F., Gardin, S., Jovane, F., Figueiredo, M., Tedeschi, L.R., Janikian, L., Almeida, R.P., Trindade, R.I.F., 2022. Astronomical tuning of the Aptian stage and its implications for age recalibrations and paleoclimatic events. *Nature Communication* **13**, :2941| <https://doi.org/10.1038/s41467-022-30075-3>.
- Li, M., Kump, L.R., Hinnov, L.A., Mann, M.E., 2018. Tracking variable sedimentation rates and astronomical forcing in Phanerozoic paleoclimate proxy series with evolutionary correlation coefficients and hypothesis testing. *Earth Planetary Science Letters* **501**, 165–179.
- Lithwick, Y., Wu, Y., 2011. Theory of secular chaos and Mercury's orbit. *Astrophys. J.* **739**, 31–49.
- Mogavero, F., Laskar, J., 2022. The origin of chaos in the Solar System through computer algebra. *Astronomy and Astrophysics* **662**, 1–16.
- Sussman, G.J., Wisdom, J., 1992. Chaotic evolution of the Solar System. *Science* **257**, 56–62.
- Vermeulen, J., 1980. Etude de la famille des *PULCHELLIIDAE*, révision de trois espèces types du Barrémien du Sud-Est de la France. *Thèse Doct. Spécial.*, **1-92**, Nice.
- Vermeulen, J., 2002. Etude stratigraphique et paléontologique de la famille des Pulchelliidae (ammonoidea, Ammonitina, Endemocerataceae). In: Laboratoire de Géologie de l'Université I de Grenoble (ed.), *Géologie Alpine*. Grenoble, France, p. 333.
- Vermeulen, J., Mascarelli, E., Borro, A., Lazarin, P., Lépinay, P., Leroy, L., 2018. La limite Hauterivien-Barrémien à Barrême, sud-est de la France. *Ann. Hist. Nat. Nice Tome XXXIII*, 23–31.
- Westermann, S., Stein, M., Matera, V., Fiet, N., Fleitmann, D., Adatte, T., Föllmi, K.B., 2013. Rapid changes in the redox conditions of the western Tethys Ocean during the early Aptian oceanic anoxic event. *Geochimica et Cosmochimica Acta* **121**, 467–486.
- Wissler, L., Weissert, H., Masse, J.P., Bulot, L., 2002. Chemostratigraphic correlation of Barremian and lower Aptian ammonite zones and magnetic reversals. *International Journal of Earth Science* **91**, 272–279.